Electronic Supplementary Material (ESI) for ChemComm.
This journal is © The Royal Society of Chemistry 2023

Supporting Information

Copper phenanthroline for selective electrochemical CO_2 reduction on carbon paper

Jiehao Du,[a] Banggui Cheng,[a] Long Jiang,[b] and Zhiji Han*,[a]

[a] *MOE Key Laboratory of Bioinorganic and Synthetic Chemistry, School of Chemistry, Sun Yat-Sen University, Guangzhou 510275, Email: hanzhiji@mail.sysu.edu.cn*

[b] *Instrumental Analysis and Research Center, Sun Yat-sen University, Guangzhou, 510275*

Table of Contents

Experimental Methods.

Materials

All chemicals and solvents were commercially available and used as obtained without further purification unless otherwise noted. Water was purified by a HHitech Ultrapure Water System with specific resistance of 18.2 MΩ•cm at 25 ºC. HPLC grade water was used for all spectroscopic and electrochemical measurements. Hydrophilic carbon paper (Toray, TGP-H-060) was purchased from Guangzhou Lige Science Co., Ltd. K_2CO_3 (99.995%) was purchased from Macklin. CO_2 (99.995%) and N_2 (99.999%) were purchased from Guangzhou Gas Co., Ltd. $K_2{}^{13}CO_3$ (^{13}C, 98%, CIL) was purchased from Qingdao Tenglong Weibo technology Co., Ltd. $^{13}CO_2$ (99.0 atom %, Aldrich) was purchased from Guangzhou Yuejia Gas Co., Ltd. $CuCl_2$, 1.10-phenanthroline (phen) and 2,9-dimethyl-1,10-phenanthroline (2,9-dmp) were purchased from Sigma Aldrich. 1,10-phenanthrolin-5-amine, **1** and **2** were purchased from Bide Pharmatech Ltd. 1-(2,4-dinitrophenyl)-pyridinium chloride[1] and *N*-tolyl pyridinium chloride[2] was synthesized according to published procedures. **3–5** were synthesized according to the methods reported in the literature. [3-5]

Preparation of 1-(1,10-phenanthrolin-5-yl)pyridin-1-ium chloride [(5-py-phen)Cl].

A solution of 1-(2,4-dinitrophenyl)-pyridinium chloride (1.69 g, 0.6 mmol) and 1,10-phenanthrolin-5-amine (0.98 g, 0.5 mmol) in ethanol (100 mL) was stirred under reflux for 48 h. After reaction, the mixture was concentrated under vacuum. The solid collected was dissolved in 2 mL methanol, and then precipitated by 20 mL diethyl ether. The precipitate was washed twice with diethyl ether and dried under vacuo, which gave a red-brown solid product (0.71 g, 48% yield). ^{1}H NMR (400 MHz, DMSO-d_6) δ 9.57-9.47 (m, 2H), 9.27 (ddd, J = 17.6, 4.3, 1.7 Hz, 2H), 9.04- 8.96 (m, 1H), 8.65 (dd, J = 8.1, 1.8 Hz, 1H), 8.61 (s, 1H), 8.55-8.45 (m, 2H), 8.00-7.89 (m, 2H), 7.84 (dd, J = 8.4, 4.3 Hz, 1H). ^{13}C NMR (101 MHz, DMSO-d_6) δ 152.80, 151.88, 148.43, 147.14, 146.22, 145.76, 137.93, 137.22, 131.10, 129.09, 126.90, 126.50, 125.06, 124.92, 123.98.

Preparation of complex 6 and 7.

$CuCl_2$ (0.14 g, 1 mmol) and (5-py-phen)Cl (0.59 g, 2 mmol) were mixed in 20 mL methanol, and heated at 60 °C for 2 h. Afterwards, the solvent was removed by rotary evaporation and the resulting solid was re-crystallized in a mixture of methanol and diethyl ether, affording a green solid as the final product **6** (0.13 g, 18%). Anal. Calcd. For $C_{34}H_{24}N_6CuCl_4{\cdot}5H_2O$: C, 50.33; H, 4.33; N, 10.33; found: C, 50.29; H, 4.22; N, 10.35. Due to the poor quality of single crystals of **6**, the Cl anion was exchanged with PF_6^- to obtain complex **7**, which gave crystals suitable for X-ray diffraction (Fig. S3B). Similar to other bis-phenanthroline Cu complexes,[3-5] the Cu center in **7** is five-coordinated by one Cl and four N atoms from the phenanthroline ligands in a distorted trigonal bipyramidal geometry. The N–Cu bond length in the range 2.003(3)– 2.220(3) and the bond angle (~120º) between the pyridinium and phenanthroline planes are similar to previously reported complexes. [6-7]

Characterization.

^{1}H and ^{13}C NMR spectra were recorded on a Bruker 400 MHz NMR spectrometer. UV–vis spectra were taken on a Thermo Scientific GENESYS 50 UV–visible spectrophotometer. ESI−MS spectra were obtained on a Thermo Scientific LTQ-XL ion trap mass spectrometer. Scanning electron microscopy (SEM) was recorded with HITACHI SU8010. High resolution transmission electron microscope (HR−TEM) measurements were performed on a JEOL JEM 22010 of 200 kV. X-ray photoelectron spectroscopy (XPS) was measured on an ESCALAB 250, Thermo Fisher Scientific, using a standard Al Kα (1484.8 eV) X-ray source and an analyzer pass energy of 15 eV. All binding energies of the XPS spectra were calibrated by C_{1s} at 284.8 eV.

X-ray crystallography.

X-ray diffraction data were collected on SuperNova singlecrystal diffractometer using the CuKα (1.54184 nm) radiation at 150 K. Absorption correction was carried out by a multiscan method. The crystal structure was solved by direct methods with SHELXT[8] program, and was refined by full-matrix leastsquare methods with SHELXL[8] program contained in the Olex2[9] suite. Weighted R factor (Rw) and the goodness of fit S were based on F2, conventional R factor(R) was based on F. Hydrogen atoms were placed with the AFIX instructions and were refined using a riding mode. Figures were drawn with Diamond software. Details can be obtained from the Cambridge Crystallographic Data Centre at www.ccdc.cam.ac.uk for CCDC accession number 2207405 and 2208240.

Electrochemical CO_2 Reduction

All electrochemical measurements were conducted on a CHI760E potentiostat with a three-electrode configuration. Linear sweep voltammetry and Cyclic voltammograms measurements were carried out using carbon paper as the working electrode, a platinum plate as the counter electrode, and an Ag/AgCl (saturated KCl) as the reference electrode in CO_2–saturated 0.1M $KHCO_3$ (pH = 6.8) with copper complexes, solutions were purged with CO_2 over 30 min before measurements. Controlled potential electrolysis were performed using a typical H-type cell with two compartments separated by an anion exchange membrane (Hangzhou Huamo Technology Co., Ltd). carbon paper or glassy carbon working electrode, before each measurement, the working electrode was cleaned thoroughly using the electrolyte solution. A platinum foil was used as the counter electrode and an Ag/AgCl (saturated KCl) was used as the reference electrode. If not mentioned otherwise, the electrolyte was a CO_2–saturated 0.1 M $KHCO_3$ aqueous solution, which was prepared by sparging a solution of K_2CO_3 (0.05 M) with CO_2 for least 65 min. The potentials were converted to the RHE scale using the following equation:

$$E_{RHE} = E_{Ag/AgCl} + 0.197 + 0.059 \times pH, \quad (1)$$

where E_{RHE} is the potential vs RHE, and $_{EAg/AgCl}$ is the (measured) potential vs Ag/AgCl reference electrode.

The gas products were analyzed by gas chromatography (Shimadzu GC-2014). A thermal conductivity detector (TCD) was used to detect H_2 and two flame ionization detectors (FID) were used to detect CO and hydrocarbons. Nitrogen was used as the

carrier gas. The oven temperature was kept at 60 ºC. The TCD detector and injection port were kept at 100 ºC and 200 ºC, respectively. The liquid products were analyzed by high performance liquid chromatography (HPLC) and ^{1}H NMR. For HPLC measurements, the electrolyte was diluted with a sulfuric acid solution (30 or 300 mM) to the appropriate concentration with pH adjusted to be lower than 7. The HPLC (Shimadzu LC-20AT) was equipped with a refractive index detector (Shimadzu RID-20A) and a HPX-87H (BIO-RAD) chromatographic column. During analysis, the temperatures of detector and column oven were kept at 40 ºC and 60 ºC, respectively. The mobile phase was 5 mM H_2SO_4 aqueous solution with a steady running rate of 0.5 mL/min. For ^{1}H NMR measurements, solutions containing 90% electrolyte and 10% D_2O (v/v) with DMSO as the internal standard were prepared and measured using a water suppression technique on a Bruker 400 MHz NMR spectrometer. Faradaic efficiency (FE) was calculated from the following equation:

$$\mathrm{FE} = \frac{nFz}{Q} \times 100\% \qquad (2)$$

where *n* is the amount of a specific product, z is the number of electrons required to reduce one molecule of a specific product, F is Faradaic constant, and Q is the total amount of charge passed. ^{13}C isotopic labeling experiments were carried out in a $^{13}CO_2$ atmosphere and $KH^{13}CO_3$ electrolyte. The gaseous products were detected by a gas chromatography mass spectrometry (GC–MS, Agilent 7890A–5975C) equipped with a J & W GS–Carbon PLOT (Agilent, number: 113–3133) column.

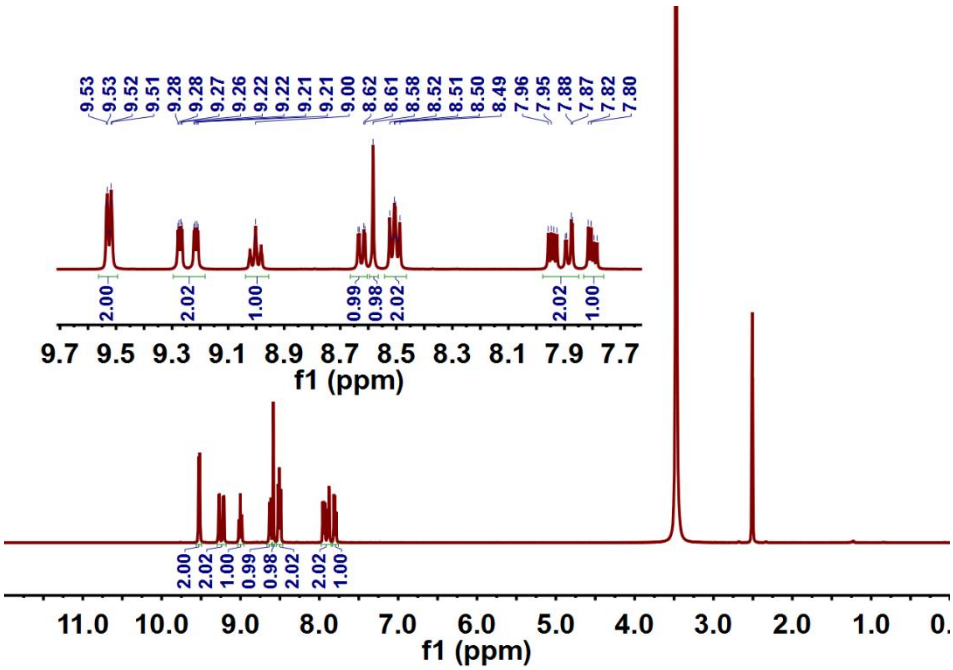

Figure S1. ^{1}H NMR spectrum of (5-py-phen)Cl in DMSO-d_6.

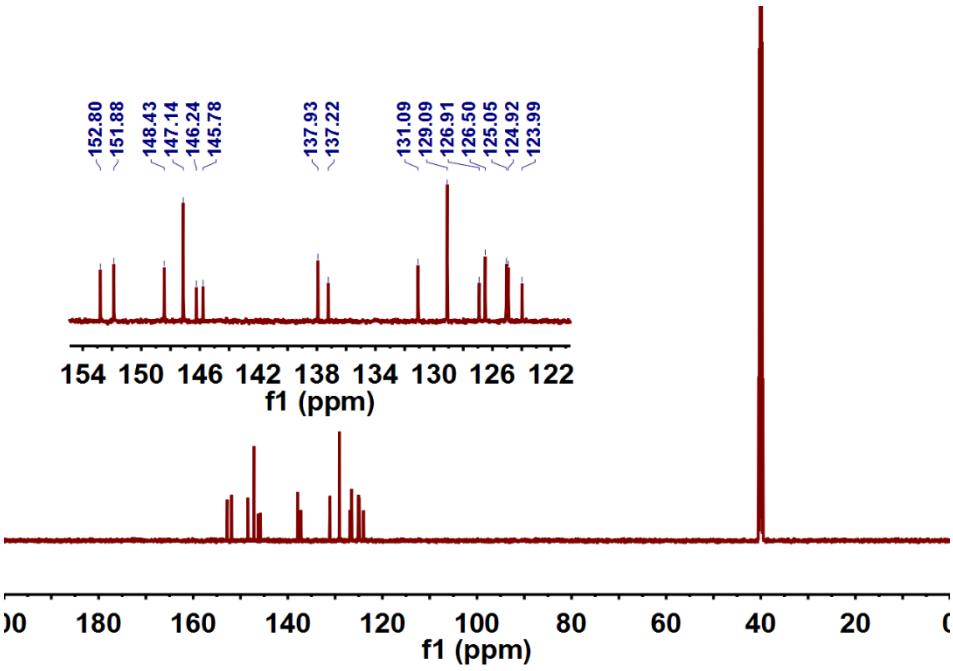

Figure S2. ^{13}C NMR spectrum of (5-py-phen)Cl in DMSO-d_6.

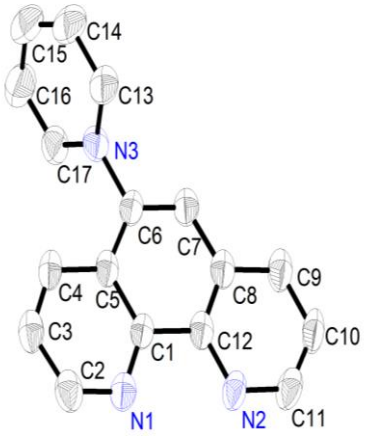

Figure S3. Thermal ellipsoid plot of (5-py-phen)Cl. Thermal ellipsoids are drawn at the 50% probability level. Hydrogen atoms and non-coordinating anions have been removed for clarity.

Table S1. Crystal data and structure refinement for (5-py-phen)Cl and **7**.

Compound	(5-py-phen)Cl	**7**
CCDC	2208240	2207405
Empirical formula	$C_{17}H_{12}ClN_3$	$C_{34}H_{24}ClCuF_{18}N_6P_3$
Formula weight	293.75	1050.50
Temperature	149.98(10) K	150 K
Wavelength	1.54184 A	1.34138 A
Crystal system, space group	Triclinic	Monoclinic
Space group	P 1	P 121/c 1
a/Å	6.9329(7)	17.2933(9)
b/Å	10.2901(14)	13.8590(7)
c/Å	11.7596(14)	15.8110(8)
α/°	98.018(11)	90
β/°	98.510(9)	94.827(2)
γ/°	96.695(10)	90
Volume/Å^3	813.48(17)	3775.9(3)
Z	2	4
Calculated density/Mg/m^3	1.199	1.8478
Absorption coefficient/mm^{-1}	2.039	5.087
F(000)	304	2091.4945
Crystal size/mm^3	0.35 x 0.12 x 0.05	0.16 x 0.08 x 0.06
Theta range for data collection/°	4.382 to 62.999	2.23 to 59.97
Limiting indices	-8<=h<=7, -7<=k<=11, -13<=l<=13	-22<=h<=22, -17<=k<=17, -19<=l<=20
Reflections collected / unique	4388 / 2544 [R(int) = 0.0395]	43524 / 8389 [R(int) = 0.0715]
Max. and min. transmission	1.00000 and 0.69294	0.7516 and 0.4659
Refinement method	Full-matrix least-squares on F^2	Full-matrix least-squares on F^2
Data / restraints / parameters	2544 / 0 / 199	8389 / 0 / 569
Goodness-of-fit on F^2	1.072	1.0350
Final R indices [I>2sigma(I)]	R1 = 0.1000, wR2 = 0.2689	R1 = 0.0585, wR2 = 0.1605
R indices (all data)	R1 = 0.1114, wR2 = 0.2833	R1 = 0.0922, wR2 = 0.1842
Largest diff. peak and hole/e Å^{-3}	0.993 and -0.375	0.9794 and -0.8505

Table S2. Selected bond lengths (Å) of (5-py-phen)Cl.

Selected bond lengths (Å)					
N(1)-C(1)	1.356(6)	C(1)-C(12)	1.458(6)	C(8)-C(12)	1.398(7)
N(1)-C(2)	1.330(6)	C(2)-C(3)	1.404(7)	C(9)-C(10)	1.371(7)
N(2)-C(11)	1.353(6)	C(3)-C(4)	1.369(6)	C(10)-C(11)	1.379(8)
N(2)-C(12)	1.357(6)	C(4)-C(5)	1.408(6)	C(13)-C(14)	1.374(7)
N(3)-C(6)	1.455(5)	C(5)-C(6)	1.431(6)	C(14)-C(15)	1.385(9)
N(3)-C(13)	1.346(6)	C(6)-C(7)	1.350(6)	C(15)-C(16)	1.382(9)
N(3)-C(17)	1.352(6)	C(7)-C(8)	1.433(6)	C(16)-C(17)	1.373(7)
C(1)-C(5)	1.422(6)	C(8)-C(9)	1.412(6)		

Table S3. Selected bond angels (°) of (5-py-phen)Cl**.**

Selected angels (°)					
C(2)-N(1)-C(1)	117.4(4)	C(1)-C(5)-C(6)	118.6(3)	C(9)-C(10)-C(11)	119.1(4)
C(11)-N(2)-C(12)	116.1(4)	C(4)-C(5)-C(1)	117.5(4)	N(2)-C(11)-C(10)	124.8(4)
C(13)-N(3)-C(6)	118.6(4)	C(4)-C(5)-C(6)	123.9(4)	N(2)-C(12)-C(1)	117.1(4)
C(13)-N(3)-C(17)	122.4(4)	C(5)-C(6)-N(3)	118.7(3)	N(2)-C(12)-C(8)	122.8(4)
C(17)-N(3)-C(6)	119.0(3)	C(7)-C(6)-N(3)	118.2(4)	C(8)-C(12)-C(1)	120.1(4)
N(1)-C(1)-C(5)	123.0(4)	C(7)-C(6)-C(5)	123.1(4)	N(3)-C(13)-C(14)	119.4(5)
N(1)-C(1)-C(12)	118.5(4)	C(6)-C(7)-C(8)	119.5(4)	C(13)-C(14)-C(15)	119.7(5)
C(5)-C(1)-C(12)	118.5(4)	C(9)-C(8)-C(7)	120.8(4)	C(16)-C(15)-C(14)	119.4(5)
N(1)-C(2)-C(3)	123.6(4)	C(12)-C(8)-C(7)	120.3(4)	C(17)-C(16)-C(15)	119.9(5)
C(4)-C(3)-C(2)	119.4(4)	C(12)-C(8)-C(9)	118.9(4)	N(3)-C(17)-C(16)	119.2(4)
C(3)-C(4)-C(5)	119.1(4)	C(10)-C(9)-C(8)	118.3(5)		

Table S4. Selected bond lengths (Å) of **7**.

Selected bond lengths (Å)					
Cu(01)-Cl(02)	2.2388(10)	Cu(01)-N(00L)	2.220(3)	Cu(01)-N(00M)	2.084(3)
Cu(01)-N(00O)	2.005(3)	Cu(01)-N(00P)	2.003(3)	N(00K)-C(00T)	1.459(4)
N(00K)-C(01E)	1.354(5)	N(00K)-C(01M)	1.329(4)	N(00L)-C(00S)	1.361(4)
N(00L)-C(016)	1.323(4)	N(00M)-C(00V)	1.361(4)	N(00M)-C(012)	1.326(4)
N(00N)-C(00W)	1.459(4)	N(00N)-C(01I)	1.341(5)	N(00N)-C(01P)	1.347(5)
N(00O)-C(00R)	1.356(4)	N(00O)-C(01O)	1.314(4)	N(00P)-C(00Z)	1.356(4)
N(00P)-C(01F)	1.333(4)				

Table S5. Selected bond angels (°) of **7.**

Selected angels (°)			
N(00L)-Cu(01)-Cl(02)	115.90(8)	N(00M)-Cu(01)-Cl(02)	153.39(8)
N(00O)-Cu(01)-Cl(02)	92.04(9)	N(00P)-Cu(01)-Cl(02)	95.19(8)
N(00M)-Cu(01)-N(00L)	90.71(10)	N(00O)-Cu(01)-N(00L)	79.06(11)
N(00O)-Cu(01)-N(00M)	93.92(12)	N(00P)-Cu(01)-N(00L)	95.19(11)
N(00P)-Cu(01)-N(00M)	80.86(11)	N(00P)-Cu(01)-N(00O)	172.24(12)
C(00S)-N(00L)-Cu(01)	109.5(2)	C(016)-N(00L)-Cu(01)	132.6(2)
C(00V)-N(00M)-Cu(01)	110.4(2)	C(012)-N(00M)-Cu(01)	130.9(2)
C(00R)-N(00O)-Cu(01)	115.9(2)	C(01O)-N(00O)-Cu(01)	124.5(2)
C(00Z)-N(00P)-Cu(01)	112.8(2)	C(01F)-N(00P)-Cu(01)	128.3(2)
C(01E)-N(00K)-C(00T)	117.4(3)	C(01M)-N(00K)-C(00T)	121.9(3)
C(01M)-N(00K)-C(01E)	120.8(3)	C(016)-N(00L)-C(00S)	117.8(3)
C(012)-N(00M)-C(00V)	117.7(3)	C(01I)-N(00N)-C(00W)	121.5(3)
C(01P)-N(00N)-C(00W)	116.7(3)	C(01P)-N(00N)-C(01I)	121.8(3)
C(01O)-N(00O)-C(00R)	119.6(3)	C(01F)-N(00P)-C(00Z)	118.2(3)
C(00S)-C(00R)-N(00O)	118.5(3)	C(00U)-C(00R)-N(00O)	120.9(3)
C(00R)-C(00S)-N(00L)	116.9(3)	C(017)-C(00S)-N(00L)	123.0(3)
C(00X)-C(00T)-N(00K)	118.9(3)	C(011)-C(00T)-N(00K)	118.0(3)
C(00Z)-C(00V)-N(00M)	116.3(3)	C(010)-C(00V)-N(00M)	123.6(3)
C(00U)-C(00W)-N(00N)	117.0(3)	C(01D)-C(00W)-N(00N)	119.4(3)
C(00V)-C(00Z)-N(00P)	116.9(3)	C(011)-C(00Z)-N(00P)	122.7(3)
C(01B)-C(012)-N(00M)	122.8(3)	C(018)-C(016)-N(00L)	123.0(3)
C(01G)-C(01E)-N(00K)	120.1(4)	C(01L)-C(01F)-N(00P)	122.8(3)
C(014)-C(01I)-N(00N)	119.2(4)	C(01N)-C(01M)-N(00K)	120.7(4)
C(01H)-C(01O)-N(00O)	122.8(3)	C(01Q)-C(01P)-N(00N)	120.0(4)

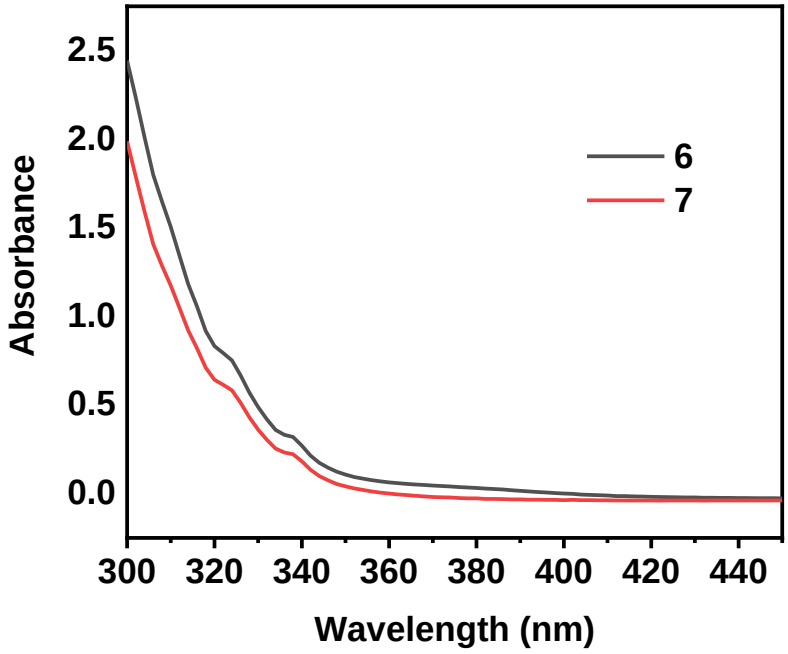

Figure S4. UV−Vis spectra of complexes **6** (grey) and **7** (red) in DMSO.

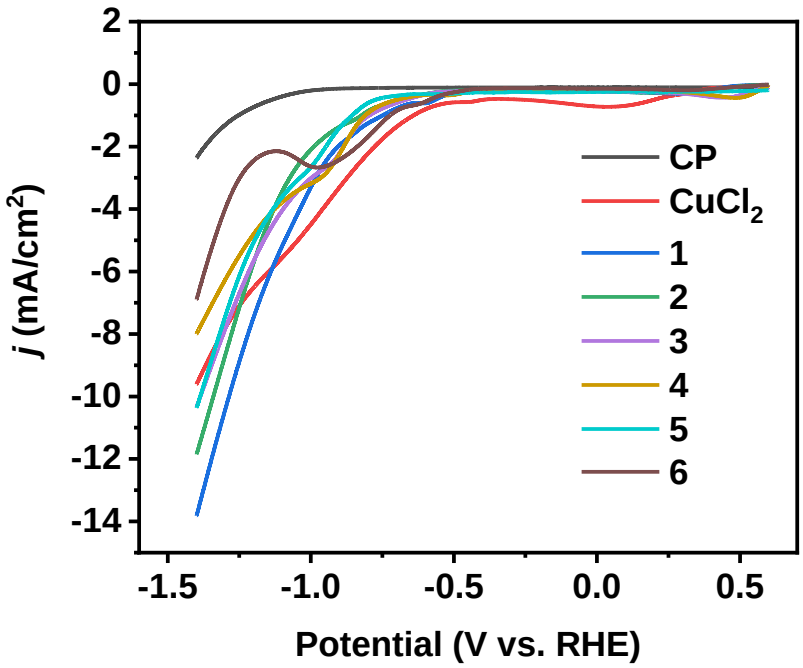

Figure S5. Linear sweep voltammetry of 1.0 mM **1**−**6** in 0.1 M $KHCO_3$ electrolyte under CO_2 on carbon paper as working electrode with a scan rate of 100 mV/s.

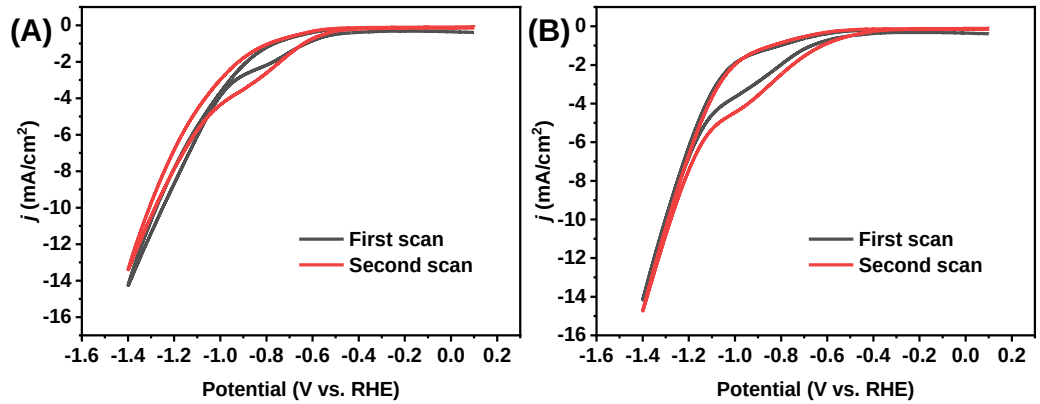

Figure S6. Cyclic voltammograms of 1.0 mM **$CuCl_2$** in 0.1 M $KHCO_3$ electrolyte under N_2 (A) and CO_2 (B) on carbon paper as working electrode with a scan rate of 100 mV/s.

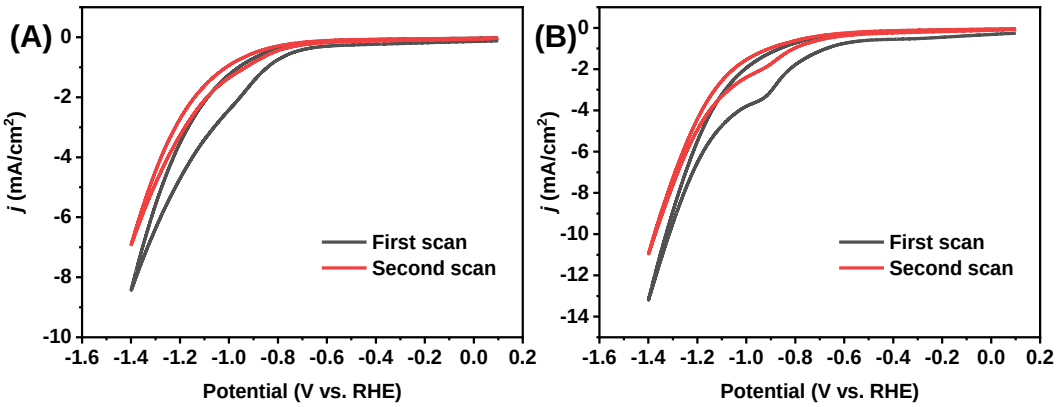

Figure S7. Cyclic voltammograms of 1.0 mM **1** in 0.1 M $KHCO_3$ electrolyte under N_2 (A) and CO_2 (B) on carbon paper as working electrode with a scan rate of 100 mV/s.

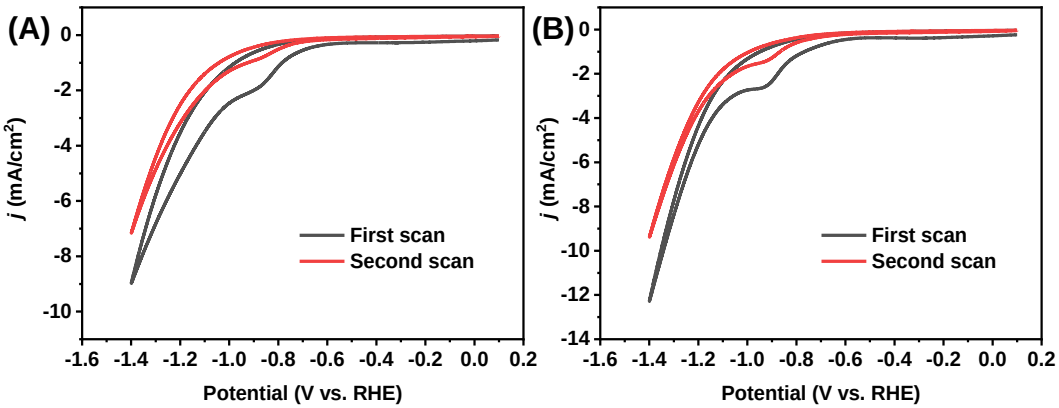

Figure S8. Cyclic voltammograms of 1.0 mM **2** in 0.1 M $KHCO_3$ electrolyte under N_2 (A) and CO_2 (B) on carbon paper as working electrode with a scan rate of 100 mV/s.

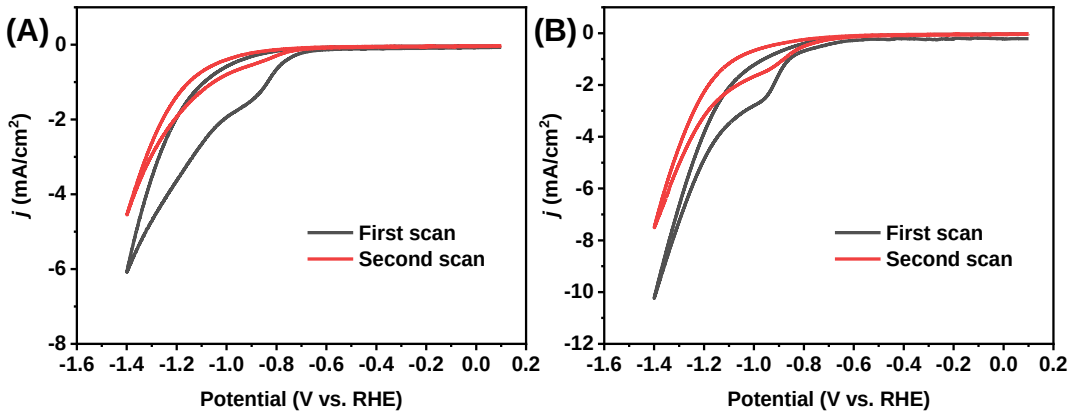

Figure S9. Cyclic voltammograms of 1.0 mM **3** in 0.1 M $KHCO_3$ electrolyte under N_2 (A) and CO_2 (B) on carbon paper as working electrode with a scan rate of 100 mV/s.

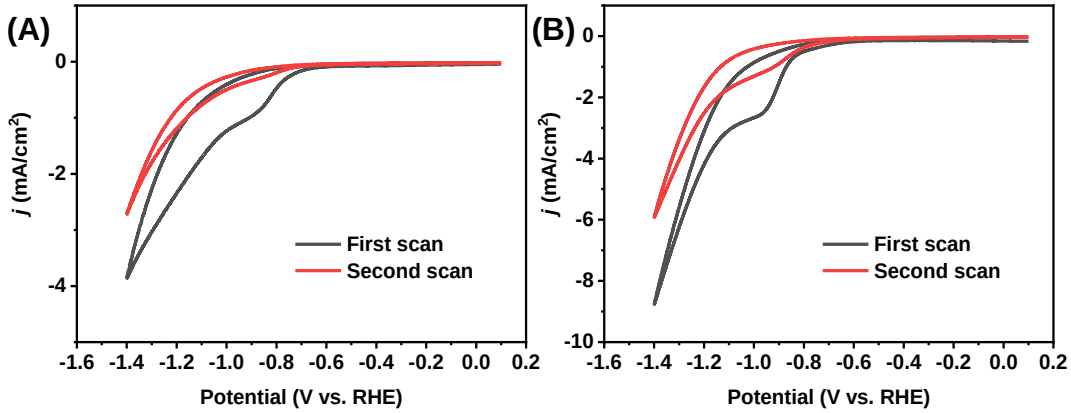

Figure S10. Cyclic voltammograms of 1.0 mM **4** in 0.1 M $KHCO_3$ electrolyte under N_2 (A) and CO_2 (B) on carbon paper as working electrode with a scan rate of 100 mV/s.

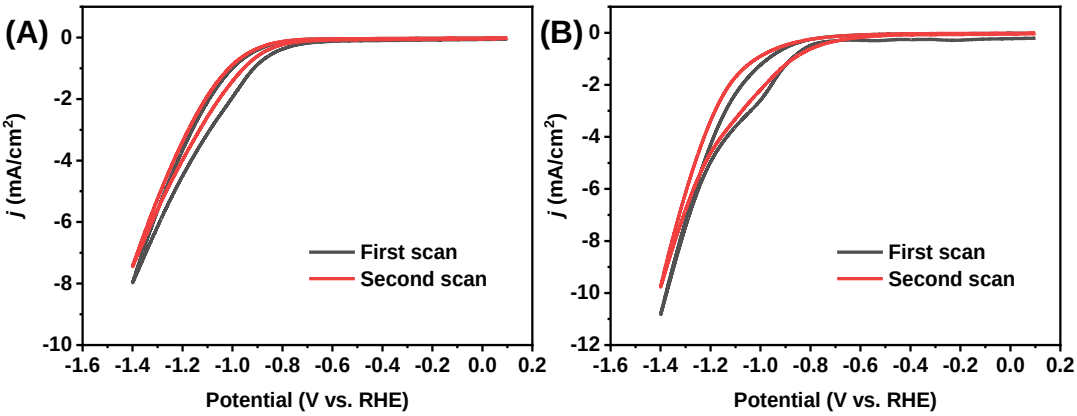

Figure S11. Cyclic voltammograms of 1.0 mM **5** in 0.1 M $KHCO_3$ electrolyte under N_2 (A) and CO_2 (B) on carbon paper as working electrode with a scan rate of 100 mV/s.

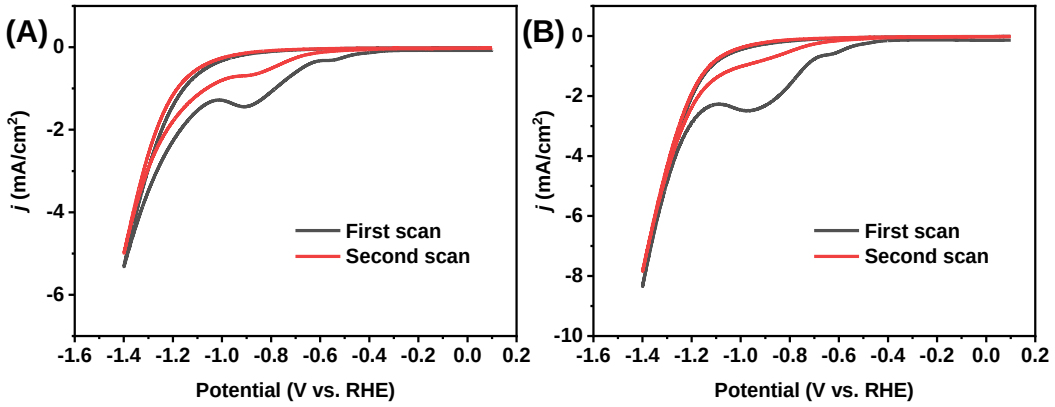

Figure S12. Cyclic voltammograms of 1.0 mM **6** in 0.1 M $KHCO_3$ electrolyte under N_2 (A) and CO_2 (B) on carbon paper as working electrode with a scan rate of 100 mV/s.

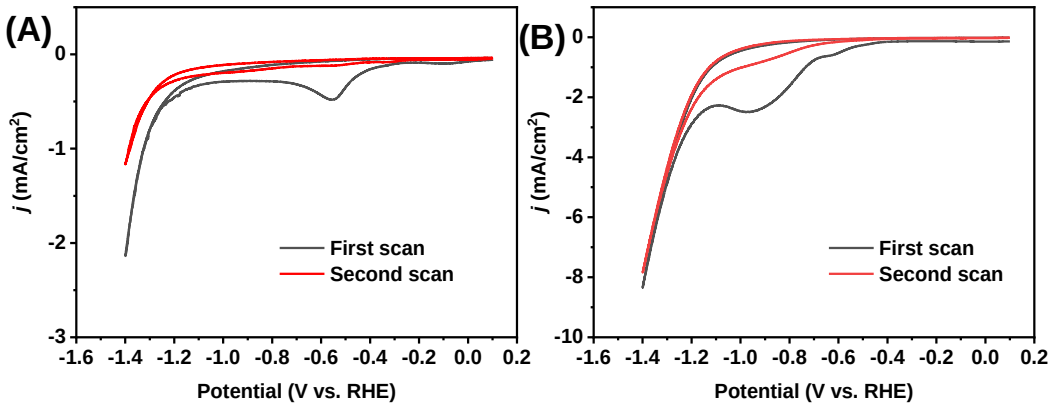

Figure S13. Cyclic voltammograms of 1.0 mM (5-py-phen)Cl (A) and **6** (B) in 0.1 M $KHCO_3$ electrolyte under CO_2 on carbon paper as working electrode with a scan rate of 100 mV/s.

Table S6. The cathodic peak potential (E_{pc}) for complexes. [a]

Complex	E_{pc}	
	N_2	CO_2
$CuCl_2$	−0.76	−0.83
1	−0.95	−0.93
2	−0.83	−0.93
3	−0.92	−0.96
4	−0.91	−0.97
5	--	−1.01
6	−0.91	−0.97

[a] All values in V vs. RHE; 1.0 mM complex with the first cathodic in 0.1 M $KHCO_3$ electrolyte on carbon paper as working electrode with a scan rate of 100 mV/s.

Table S7. Faradaic efficiencies toward different products produced during CO_2 reduction with 1.0 mM different pre-catalysts. Electrolysis was conducted in a CO_2-saturated 0.1 M $KHCO_3$ electrolyte at an applied potential of −1.3 V_{RHE} for 2 h.[a]

Pre-catalyst	FE (%)											*j*
	H_2	CO	HCOOH	CH_4	C_2H_4	C_2H_6	C_2H_5OH	C_3H_6	C_3H_7OH	C_{2+}	Total	(mA/cm^2)
None	85.6	6.0	0	0	0	0	0	0	0	0	91.6	1.3
Phen	83.2	3.4	0	0	0	0	0	0	0	0	86.6	1.0
$CuCl_2$	62.3	6.9	14.0	0.4	6.0	0.5	0.4	0.1	1.5	8.5	92.1	14.1
1	35.3	27.5	6.2	5.7	12.2	0.2	3.4	0	0	15.8	90.5	8.8
2	19.7	30.4	6.8	2.9	27.1	0.7	2.1	0.1	0	30	89.8	4.5
3	8.0	18.2	2.7	2.2	62.2	0.1	3.2	0.1	1.5	67.1	98.2	7.2
4	7.7	12.5	4.5	2.6	68.5	0.1	2.6	0.1	0.9	72.2	99.5	6.6
5	13.4	31.0	7.1	8.5	31.7	0	2.5	0	0	34.2	94.2	2.1
6	7.0	16.9	9.5	10.8	14.7	0	37.1	0	0	51.8	96.0	2.5
4[b]	90.5	0	0	0	0	0	0	0	0	0	90.5	2.3

[a] All values are an average of at least three runs. [b] Nitrogen atmosphere.

Table S8. Summary of molecular metal complexes for electrocatalytic CO_2 reduction to C_{2+}.

Entry	Supporting electrode	Catalyst	Potential (V vs. RHE)	Electrolyte	FE (%) for C_{2+} product	Reference
1	Graphene−coated carbon paper	$Cu(phen)_2$	−1.0	0.1 M $KHCO_3$	C_2H_4 (2.4)	10
2	Carbon paper	PorCu	−0.976	0.5 M $KHCO_3$	C_2H_4 (17)	11
3	Carbon paper	Crystalline CuPc	−1.0	0.5 M KCl	C_2H_4 (25)	12
4	Graphitized mesoporous carbon coated carbon paper	$[Cu_2(NTB)_2]$	−1.278	0.1 M KCl	C_2H_4 (42)	13
5	Coated graphite	Cu-Salen	−1.2	0.5 M $KHCO_3$, pH = 7	C_2H_5OH (15.2) CH_3COOH (14.0)	14
6	Ketjen black	Bicentric Cu porphyrin	−1.2	0.1M $KHCO_3$	C_2H_5OH (32.5) *n*-C_3H_7OH (18.3)	15
7	Graphite plate	Ni-Salen	−1.2	0.5 M $KHCO_3$, pH = 7	C_2H_5OH (28.6) CH_3CHO (4.7)	16
8	Carbon paper	Co-corrole	−0.8	0.1 M $NaClO_4$ pH = 6 phosphate buffer.	CH_3CH_2OH (48) CH_3COOH (10)	17
9	Carbon paper	Mn-corrole	−0.7	0.1 M phosphate buffer, pH = 6	CH_3COOH (63)	18
10	N-doped porous carbon	Ru polypyridyl carbene	−1.17 vs NHE	0.5M $KHCO_3$	C_2H_5OH (27.5) CH_3COOH (12.5)	19
11	Carbon paper	**4**	−1.3	0.1 M $KHCO_3$,	C_2H_4 (71.2) C_2H_5OH (1.7) *n*-C_3H_7OH (1.2)	This work
12	Carbon paper	**6**			C_2H_4 (14.7) C_2H_5OH (37.1)	

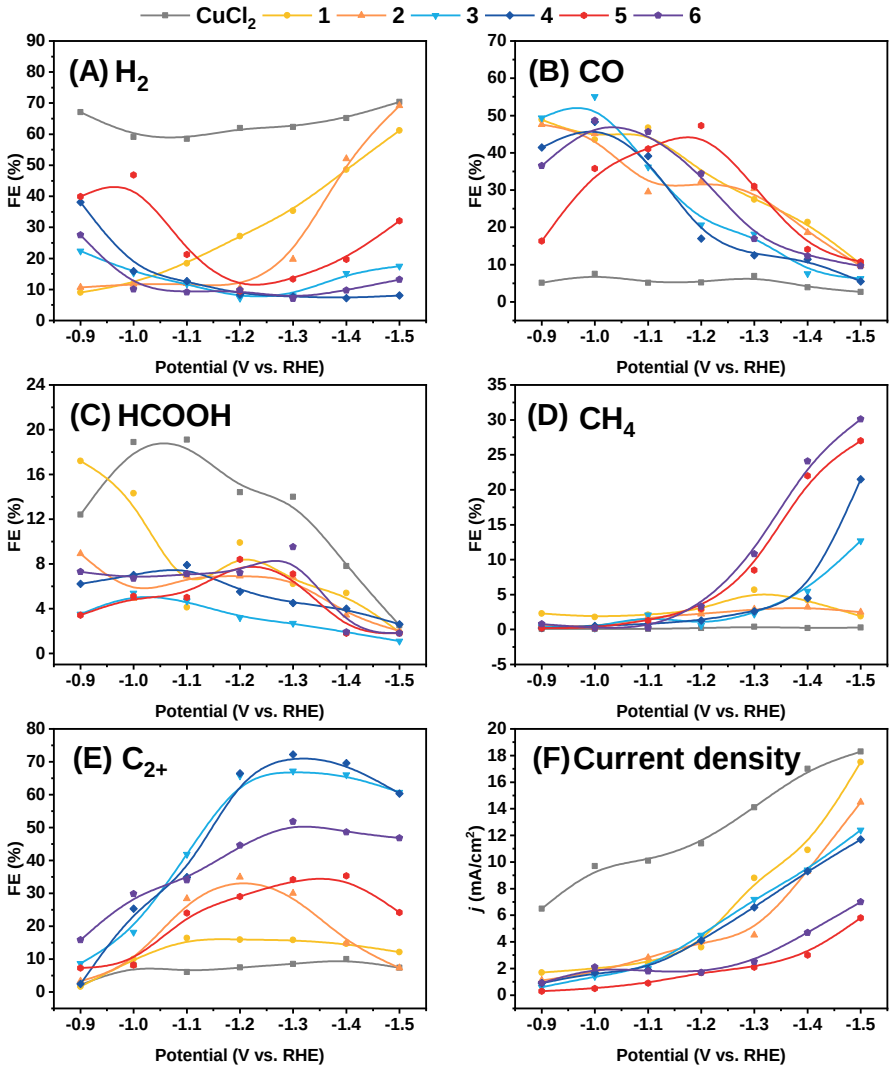

Figure S14. Faradaic efficiencies (A) H_2, (B) CO, (C) HCOOH, (D) CH_4, (E) C_{2+} and (F) current density of CO_2 reduction with different pre-catalyst at different applied potentials. Electrolysis was conducted in a CO_2-saturated 0.1 M $KHCO_3$ electrolyte for 2 h.

Table S9. Faradaic efficiencies toward different products produced during CO_2 reduction with 1.0 mM $CuCl_2$ as the pre-catalyst at different applied potentials. Electrolysis was conducted in a CO_2-saturated 0.1 M $KHCO_3$ electrolyte for 2 h.

Potential (V	FE (%)											*j*
vs RHE)	H_2	CO	HCOOH	CH_4	C_2H_4	C_2H_6	C_2H_5OH	C_3H_6	C_3H_7OH	C_{2+}	Total	(mA/cm^2)
−0.9	67.1	5.1	12.4	0.1	1.9	0.1	0	0.2	0	2.2	86.9	6.5
−1.0	59.1	7.5	18.9	0.1	6.8	0.4	0	0.1	0.9	8.2	93.8	9.7
−1.1	58.5	5.1	19.1	0.1	5.3	0.2	0	0.1	0.5	6.1	88.9	10.1
−1.2	62.0	5.2	14.4	0.2	6.7	0.3	0.2	0.1	0.2	7.5	89.3	11.4
−1.3	62.3	6.9	14.0	0.4	6.0	0.5	0.4	0.1	1.5	8.5	92.1	14.1
−1.4	65.2	3.9	7.8	0.2	8.2	0.4	0.2	0.1	1.1	10.0	87.1	17.0
−1.5	70.4	2.7	2.5	0.3	6.4	0.2	0.2	0	0.6	7.4	83.3	18.3

Table S10. Faradaic efficiencies toward different products produced during CO_2 reduction with 1.0 mM **1** as the pre-catalyst at different applied potentials. Electrolysis was conducted in a CO_2-saturated 0.1 M $KHCO_3$ electrolyte for 2 h.

Potential (V	FE (%)											*j*
vs RHE)	H_2	CO	HCOOH	CH_4	C_2H_4	C_2H_6	C_2H_5OH	C_3H_6	C_3H_7OH	C_{2+}	Total	(mA/cm^2)
−0.9	9.0	48.9	17.2	2.3	1.6	0	0	0	0	1.6	79	1.7
−1.0	11.9	43.5	14.3	1.8	9.4	0.1	0.5	0	0	10.0	81.5	2.0
−1.1	18.4	46.7	4.1	2.1	14.7	0.3	1.4	0	0	16.4	87.7	2.4
−1.2	27.2	34.5	9.9	2.7	12.7	0.7	2.5	0	0	15.9	90.2	3.6
−1.3	35.3	27.5	6.2	5.7	12.2	0.2	3.4	0	0	15.8	90.5	8.8
−1.4	48.6	21.4	5.4	4.2	11.8	0.2	2.7	0	0	14.7	94.3	10.9
−1.5	61.2	10.1	1.9	1.9	10.6	0.2	1.3	0	0	12.1	87.2	17.5

Table S11. Faradaic efficiencise toward different products produced during CO_2 reduction with 1.0 mM **2** as the pre-catalyst at different applied potentials. Electrolysis was conducted in a CO_2-saturated 0.1 M $KHCO_3$ electrolyte for 2 h.

Potential (V	FE (%)											*j*
vs RHE)	H_2	CO	HCOOH	CH_4	C_2H_4	C_2H_6	C_2H_5OH	C_3H_6	C_3H_7OH	C_{2+}	Total	(mA/cm^2)
−0.9	10.7	47.6	8.9	0.6	3.2	0.1	0	0	0	3.3	71.1	1.1
−1.0	11.7	45.1	4.9	0.3	8.1	0.1	0	0	0	8.2	70.2	1.7
−1.1	11.9	29.5	6.9	1.8	26.0	0.3	2.0	0.1	0	28.4	78.5	2.8
−1.2	10.4	32.3	6.9	2.2	31.9	0.4	2.5	0.1	0	34.9	86.7	4.0
−1.3	19.7	30.4	6.8	2.9	27.1	0.7	2.1	0.1	0	30.0	89.8	4.5
−1.4	52.1	18.6	3.4	3.2	13.0	0.6	1.1	0.1	0	14.8	92.1	9.3
−1.5	69.2	9.7	2.0	2.5	6.5	0.3	0.3	0.2	0	7.3	90.7	14.5

Table S12. Faradaic efficiencies toward different products produced during CO_2 reduction with 1.0 mM **3** as the pre-catalyst at different applied potentials. Electrolysis was conducted in a CO_2-saturated 0.1 M $KHCO_3$ electrolyte for 2 h.

Potential (V	FE (%)											*j*
vs RHE)	H_2	CO	HCOOH	CH_4	C_2H_4	C_2H_6	C_2H_5OH	C_3H_6	C_3H_7OH	C_{2+}	Total	(mA/cm^2)
−0.9	22.4	49.4	3.5	0.4	4.1	0	0	0	4.6	8.7	84.4	0.6
−1.0	15.4	55.1	5.4	0.2	17.1	0	0	0	1.1	18.2	94.2	1.4
−1.1	11.8	36.2	4.7	2.1	37.2	0.1	1.1	0	3.5	41.9	96.7	2.0
−1.2	7.2	20.7	3.2	0.6	61.6	0.1	2.4	0.1	1.5	65.7	97.4	4.5
−1.3	8.0	18.2	2.7	2.2	62.2	0.1	3.2	0.1	1.5	67.2	98.2	7.2
−1.4	15.2	7.6	1.9	5.5	61.1	0.1	1.8	0.1	3.0	66.1	96.3	9.4
−1.5	17.5	6.3	1.1	12.7	56.7	0.1	1.3	0.1	2.6	60.7	98.4	12.4

Table S13. Faradaic efficiencies toward different products produced during CO_2 reduction with 1.0 mM **4** as the pre-catalyst at different applied potentials. Electrolysis was conducted in a CO_2-saturated 0.1 M $KHCO_3$ electrolyte for 2 h.

Potential (V	FE (%)											*j*
vs RHE)	H_2	CO	HCOOH	CH_4	C_2H_4	C_2H_6	C_2H_5OH	C_3H_6	C_3H_7OH	C_{2+}	Total	(mA/cm^2)
−0.9	38.1	41.4	6.2	0.2	2.5	0	0	0	0	2.5	88.4	0.9
−1.0	15.9	48.3	7.0	0.5	25.3	0	0	0	0	25.3	97.0	1.7
−1.1	12.7	39.1	7.9	0.8	31.7	0	3.1	0	0.1	34.9	95.4	1.9
−1.2	8.3	17.0	5.5	1.3	61.5	0.1	4.1	0	0.8	66.5	98.6	4.1
−1.3	7.7	12.5	4.5	2.6	68.5	0.1	2.6	0.1	0.9	72.2	99.5	6.6
−1.4	7.2	11.4	4.0	4.5	65.8	0.1	2.4	0.1	1.2	69.6	96.7	9.3
−1.5	8.1	5.5	2.6	21.5	58.8	0	1.1	0	0.4	60.3	98.0	11.7

Table S14. Faradaic efficiencies toward different products produced during CO_2 reduction with 1.0 mM **5** as the pre-catalyst at different applied potentials. Electrolysis was conducted in a CO_2-saturated 0.1 M $KHCO_3$ electrolyte for 2 h.

Potential (V	FE (%)											*j*
vs RHE)	H_2	CO	HCOOH	CH_4	C_2H_4	C_2H_6	C_2H_5OH	C_3H_6	C_3H_7OH	C_{2+}	Total	(mA/cm^2)
−0.9	39.9	16.3	3.4	0.2	7.0	0	0.3	0	0	7.3	67.1	0.3
−1.0	46.9	35.8	5.1	0.2	7.6	0	0.6	0	0	8.2	96.2	0.5
−1.1	21.3	41.1	5.0	1.3	23.2	0.1	0.7	0	0	24.0	92.7	0.9
−1.2	9.5	47.3	8.4	3.0	27.3	0.1	1.6	0	0	29.0	97.2	1.7
−1.3	13.4	31.0	7.1	8.5	31.7	0	2.5	0	0	34.2	94.2	2.1
−1.4	19.7	14.1	1.8	22.0	34.3	0	1.0	0	0	35.3	92.9	3.0
−1.5	32.1	10.8	1.8	27.0	23.5	0	0.7	0	0	24.2	95.9	5.8

Table S15. Faradaic efficiencies toward different products produced during CO_2 reduction with 1.0 mM **6** as the pre-catalyst at different applied potentials. Electrolysis was conducted in a CO_2-saturated 0.1 M $KHCO_3$ electrolyte for 2 h.

Potential (V	FE (%)											*j*
vs RHE)	H_2	CO	HCOOH	CH_4	C_2H_4	C_2H_6	C_2H_5OH	C_3H_6	C_3H_7OH	C_{2+}	Total	(mA/cm^2)
−0.9	27.5	36.5	7.3	0.8	3.7	0	12.1	0	0	15.8	88.0	0.9
−1.0	10.1	48.7	6.7	0.2	5.0	0	24.8	0	0	29.8	95.5	2.1
−1.1	9.1	45.6	7.1	0.2	5.6	0	28.4	0	0	34.0	95.9	1.8
−1.2	9.8	34.4	7.2	3.3	14.2	0	30.4	0	0	44.6	99.3	1.7
−1.3	7.0	16.9	9.5	10.8	14.7	0	37.1	0	0	51.8	96.0	2.5
−1.4	9.7	12.3	1.9	24.1	26.8	0	21.8	0	0	48.6	96.6	4.7
−1.5	13.2	9.6	1.8	30.1	27.0	0	19.8	0	0	46.8	101.6	7.0

Table S16. Faradaic efficiencies toward different products produced during CO_2 reduction with **4** at different concentration. Electrolysis was conducted in a CO_2-saturated 0.1 M $KHCO_3$ electrolyte at −1.3 V_{RHE} for 2 h.

Concentration	Faradaic efficiencies (%)											*j*
(mM)	H_2	CO	HCOOH	CH_4	C_2H_4	C_2H_6	C_2H_5OH	C_3H_6	C_3H_7OH	C_{2+}	Total	(mA/cm^2)
0.1	8.0	37.6	5.0	0.4	45.3	0.1	1.5	0.1	0.8	47.8	98.8	3.5
0.5	8.1	10.5	3.1	3.3	71.2	0.1	1.7	0.1	1.2	74.3	99.3	5.4
1.0	7.7	12.5	4.5	2.6	68.5	0.1	2.6	0.1	0.9	72.2	99.5	6.6
5.0	7.7	18.2	4.0	0.6	58.3	0.1	2.4	0.1	1.1	62.0	92.5	8.0

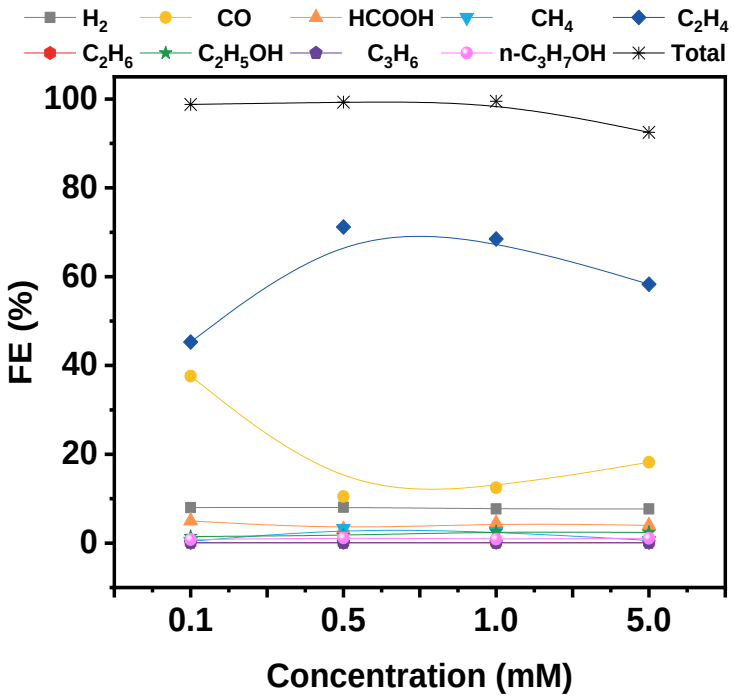

Figure S15. Faradaic efficiencies toward different products produced during CO_2 reduction with **4** at different concentration. Electrolysis was conducted in a CO_2-saturated 0.1 M $KHCO_3$ electrolyte at −1.3 V_{RHE} for 2 h.

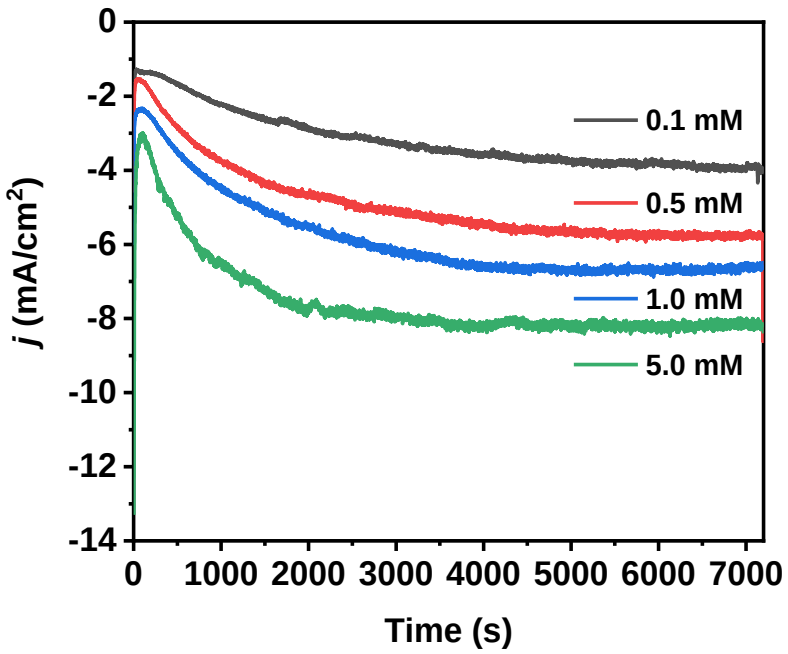

Figure S16. Chronoamperograms of electrolysis using a carbon paper electrode in a CO_2-saturated 0.1 M $KHCO_3$ electrolyte with **4** at different concentration at −1.3 V_{RHE} for 2 h.

Table S17. Faradaic efficiencies toward different products produced during CO_2 reduction used GC electrode with 1.0 mM different pre-catalysts. Electrolysis was conducted in a CO_2-saturated 0.1 M $KHCO_3$ electrolyte at an applied potential of −1.3 V_{RHE} for 2 h.

Pre-catalyst	FE (%)											*j*
	H_2	CO	HCOOH	CH_4	C_2H_4	C_2H_6	C_2H_5OH	C_3H_6	C_3H_7OH	C_{2+}	Total	(mA/cm^2)
1	39.4	21.0	1.8	1.3	26.7	0.1	2.6	0	0	29.4	92.9	8.3
2	19.4	29.3	3.0	10.5	34.0	0.4	0	0	1.7	50.1	98.3	6.0
3	4.8	11.2	3.8	11.0	62.1	0.1	2.2	0	0.9	65.3	96.1	6.5
4	6.2	18.1	4.5	2.0	65.5	0.1	1.8	0.1	1.1	68.6	99.4	7.1

Table S18. Faradaic efficiencies toward different products produced during CO_2 reduction with 1.0 mM **4** as the pre-catalyst at long time. Electrolysis was conducted in a CO_2-saturated 0.1 M $KHCO_3$ electrolyte at an applied potential of −1.3 V_{RHE}. [a]

Time (h)	FE (%)										
	H_2	CO	HCOOH	CH_4	C_2H_4	C_2H_6	C_2H_5OH	C_3H_6	C_3H_7OH	C_{2+}	Total
1	6.3	11.5	N.A.	3.1	69.1	0.1	N.A.	0.1	N.A.	69.3	90.2
2	7.2	12.8	N.A.	2.7	68.0	0.1	N.A.	0.1	N.A.	68.2	90.9
4	12.8	9.6	N.A.	2.1	64.5	0.1	N.A.	0.0	N.A.	64.5	89.1
7	13.6	12.1	N.A.	1.8	61.8	0.1	N.A.	0.1	N.A.	62.0	89.5
10	12.5	12.2	N.A.	1.5	62.0	0.1	N.A.	0.1	N.A.	62.2	88.4
13	10.9	8.5	N.A.	1.5	65.1	0.1	N.A.	0.1	N.A.	65.3	86.2
18	12.3	9.1	N.A.	1.1	64.9	0.1	N.A.	0.1	N.A.	65.1	87.6
21	22.0	12.1	N.A.	0.6	52.3	0.1	N.A.	0.1	N.A.	52.5	87.2
23	27.9	13.9	N.A.	0.2	48.1	0.2	N.A.	0.2	N.A.	48.5	90.5
28	27.5	13.2	N.A.	0.1	44.5	0.1	N.A.	0.1	N.A.	44.7	85.5
30	28.2	14.0	5.0	0.1	41.5	0.1	2.5	0.1	1.6	45.8	93.1

[a]All values are an average of at least three runs. N.A.:no application.

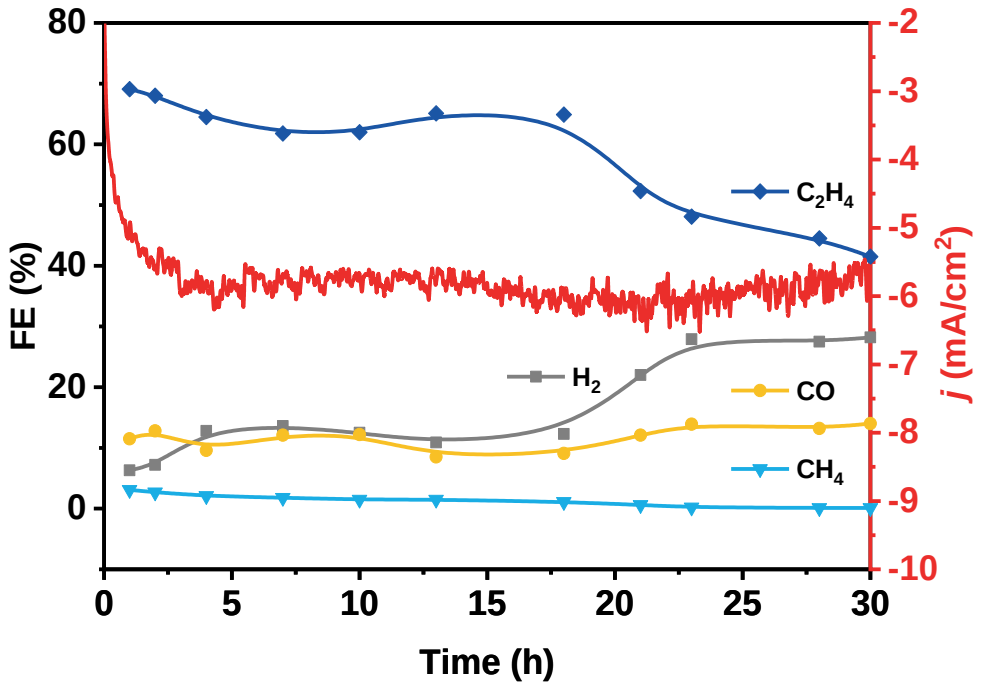

Figure S17. Chronoamperometric i–t curve and faradaic efficiencies toward different products produced during CO_2 reduction with 1.0 mM **4** as the pre-catalyst. Electrolysis was conducted in a CO_2-saturated 0.1 M $KHCO_3$ electrolyte at an applied potential of −1.3 V_{RHE} for 30h.

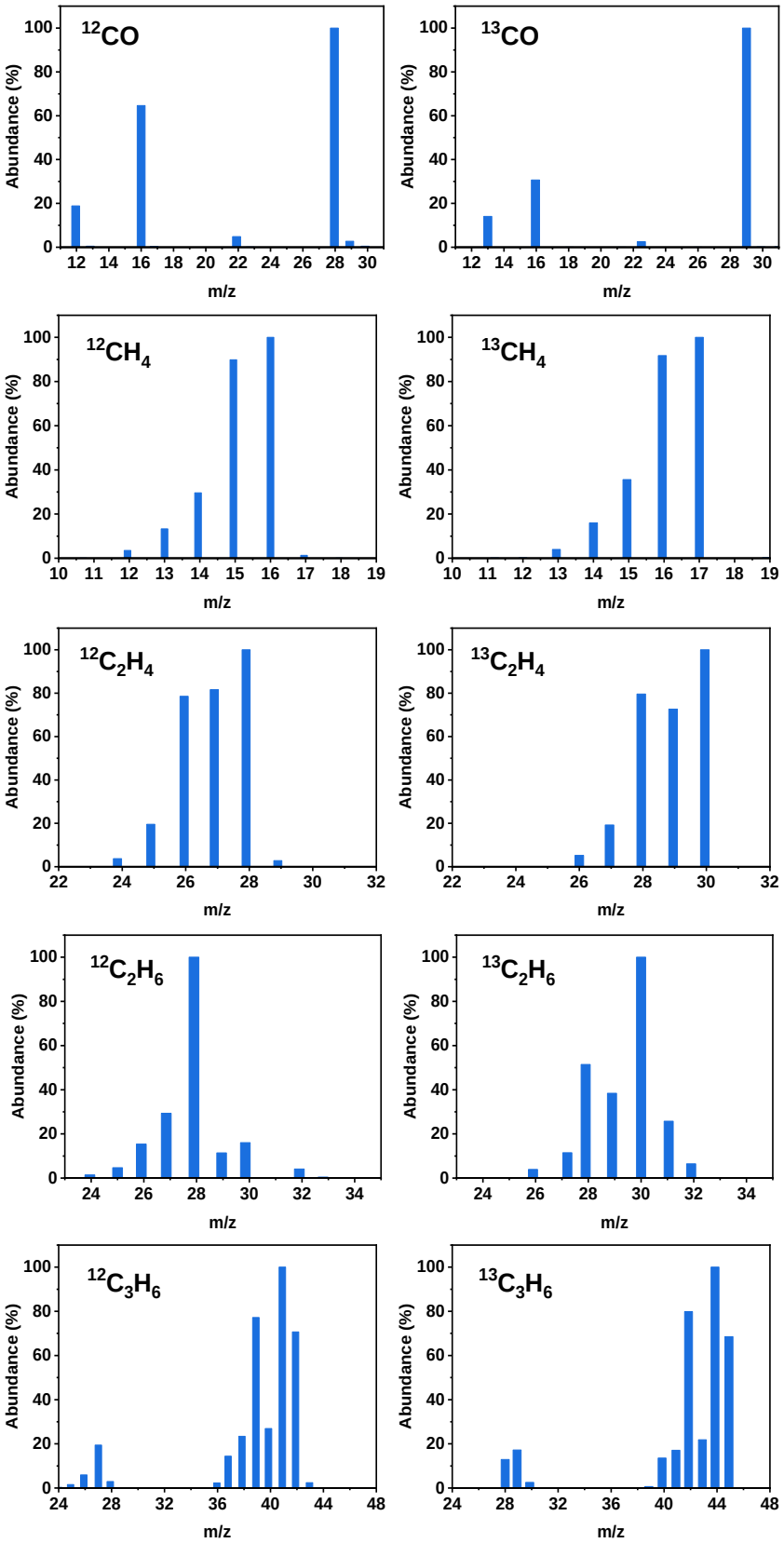

Figure S18. GC−MS measurements of calibration standard and gas products from electrolysis conducted in $^{12}CO_2$-saturated 0.1 M $KH^{12}CO_3$ electrolyte, or in $^{13}CO_2$-saturated 0.1 M $KH^{13}CO_3$ electrolyte, using 1.0 mM **4** as the pre-catalyst at an applied potential of −1.3 V_{RHE}.

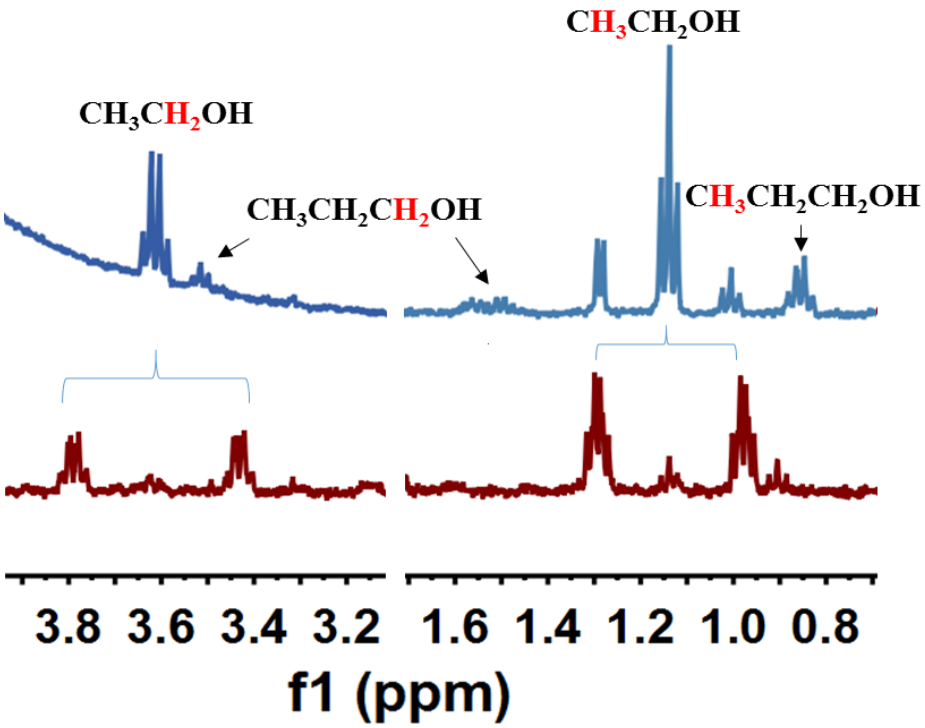

Figure S19. ^{1}H NMR spectra (400 MHz, H_2O:D_2O = 9:1) of C_2H_5OH and C_3H_7OH after electrolysis at −1.3 V_{RHE} with **4** (1.0 mM) in ^{12}C (blue) or ^{13}C-enriched (brown) CO_2-saturated $KHCO_3$.

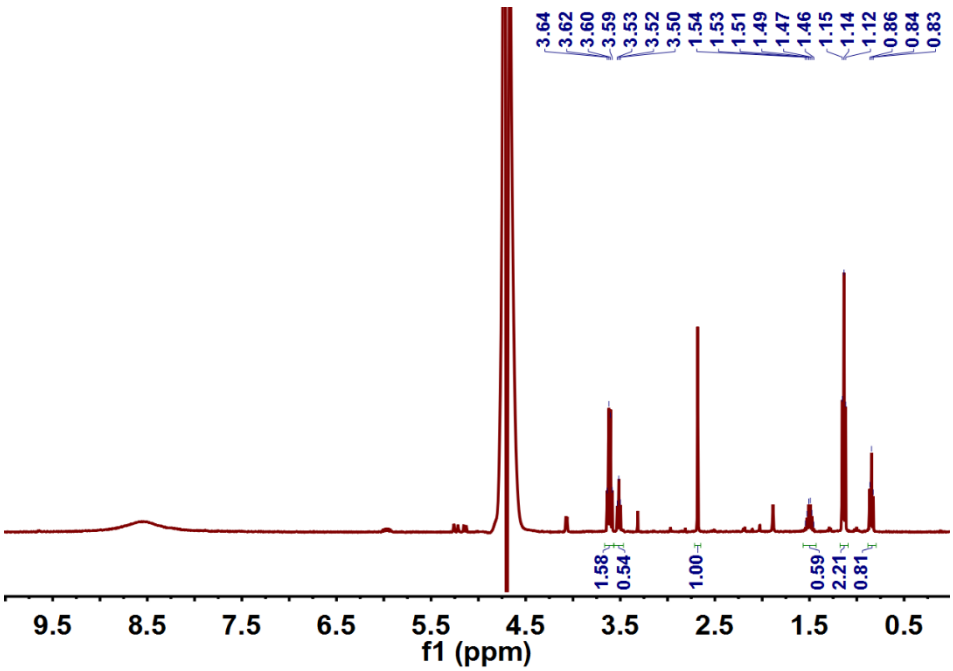

Figure S20. ^{1}H NMR spectra (400 MHz, H_2O:D_2O = 9:1, DMSO as the internal standard) of the electrolyte solution. Electrolysis was conducted in a CO_2-saturated 0.1 M $KHCO_3$ electrolyte with 1.0 mM **4** at an applied potential of −1.3 V_{RHE} for 30 h.

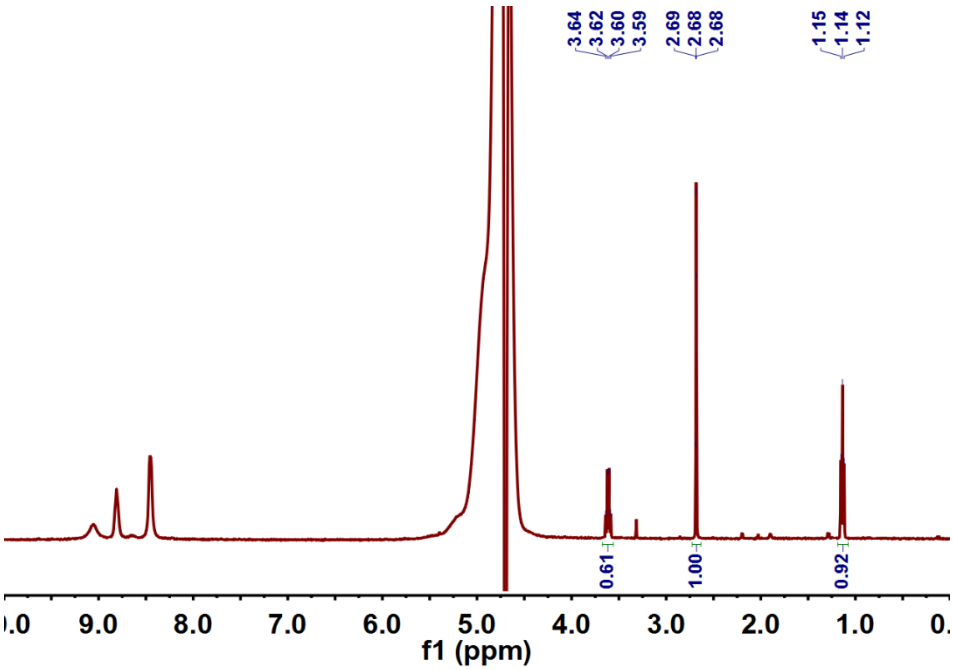

Figure S21. ^{1}H NMR spectra (400 MHz, H_2O:D_2O = 9:1, DMSO as the internal standard) of the electrolyte solution. Electrolysis was conducted in a CO_2-saturated 0.1 M $KHCO_3$ electrolyte with 1.0 mM **6** at an applied potential of −1.3 V_{RHE} for 2h.

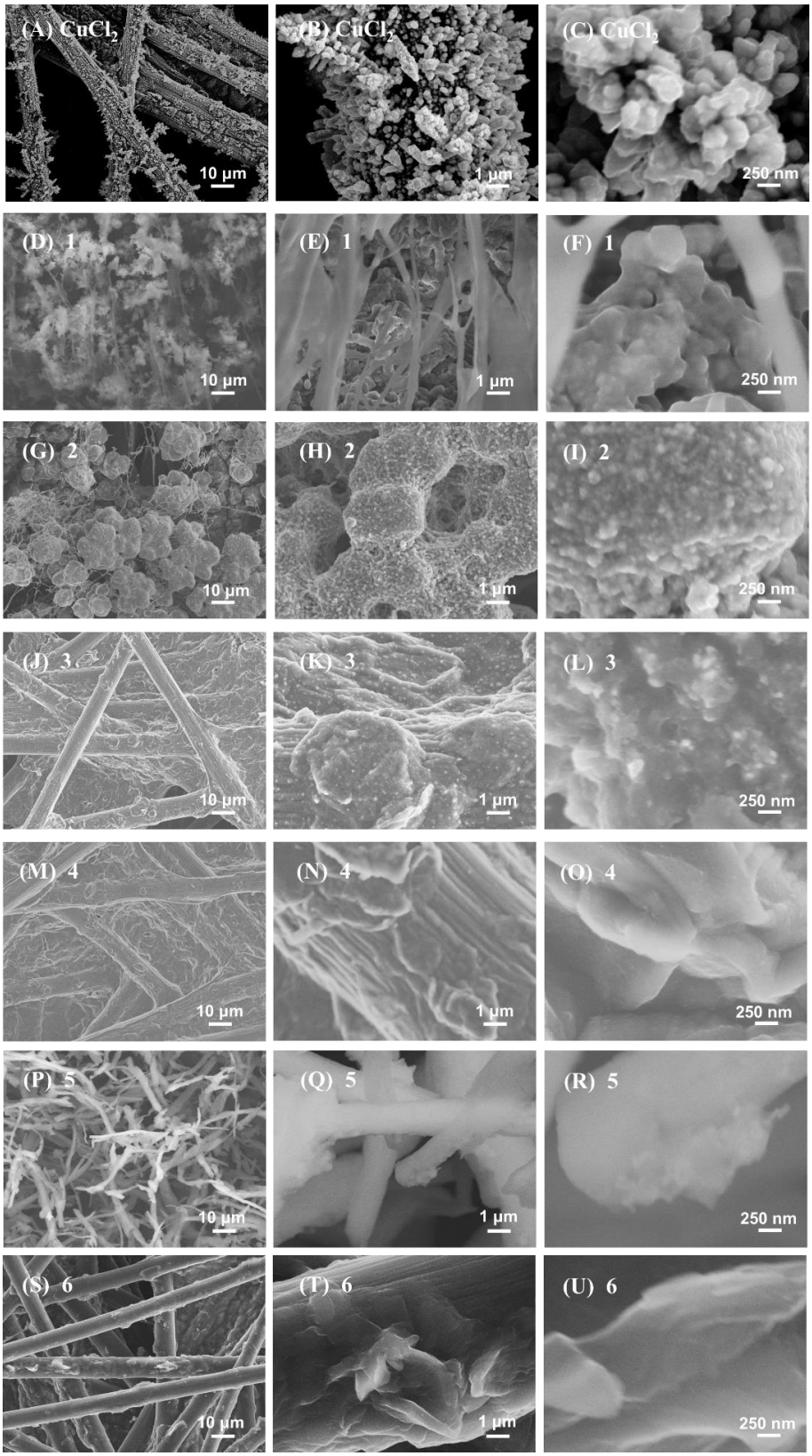

Figure S22. SEM images of carbon paper electrodes after electrolysis. (A−C) $CuCl_2$, (D−F) **1**, (G−I) **2**, (J−L) **3**, (M−O) **4**, (P−R) **5** and (S−U) **6**. Electrolysis was conducted in a CO_2-saturated 0.1 M $KHCO_3$ electrolyte with 1.0 mM different pre-catalysts at an applied potential of −1.3 V_{RHE} for 2 h.

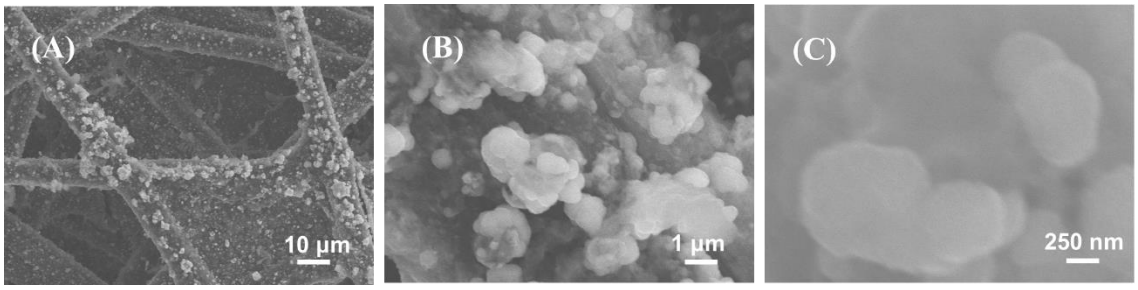

Figure S23. SEM images of carbon paper electrodes after electrolysis. Electrolysis was conducted in a CO_2-saturated 0.1 M $KHCO_3$ electrolyte with 1.0 mM **4** at an applied potential of −1.3 V_{RHE} for 30 h.

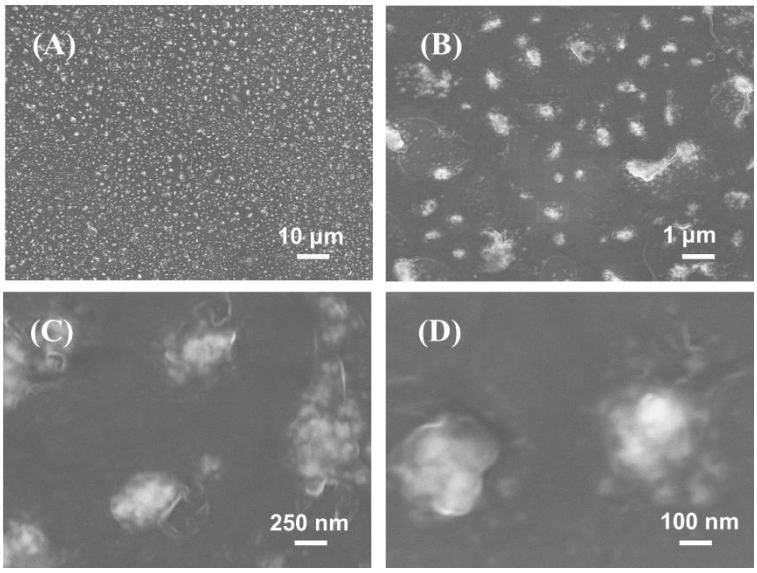

Figure S24. SEM images of GC electrodes after electrolysis. Electrolysis was conducted in a CO_2-saturated 0.1 M $KHCO_3$ electrolyte with 1.0 mM **4** at an applied potential of −1.3 V_{RHE} for 2 h.

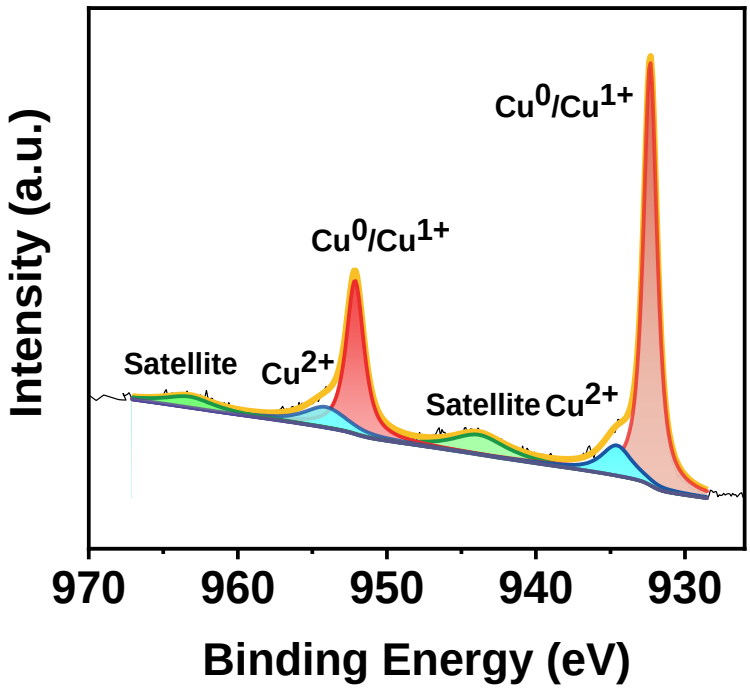

Figure S25. Cu_{2p} XPS spectra of after electrolysis with 1.0 mM $CuCl_2$. Electrolysis was conducted in a CO_2-saturated 0.1 M $KHCO_3$ electrolyte at an applied potential of −1.3 V_{RHE} for 2 h.

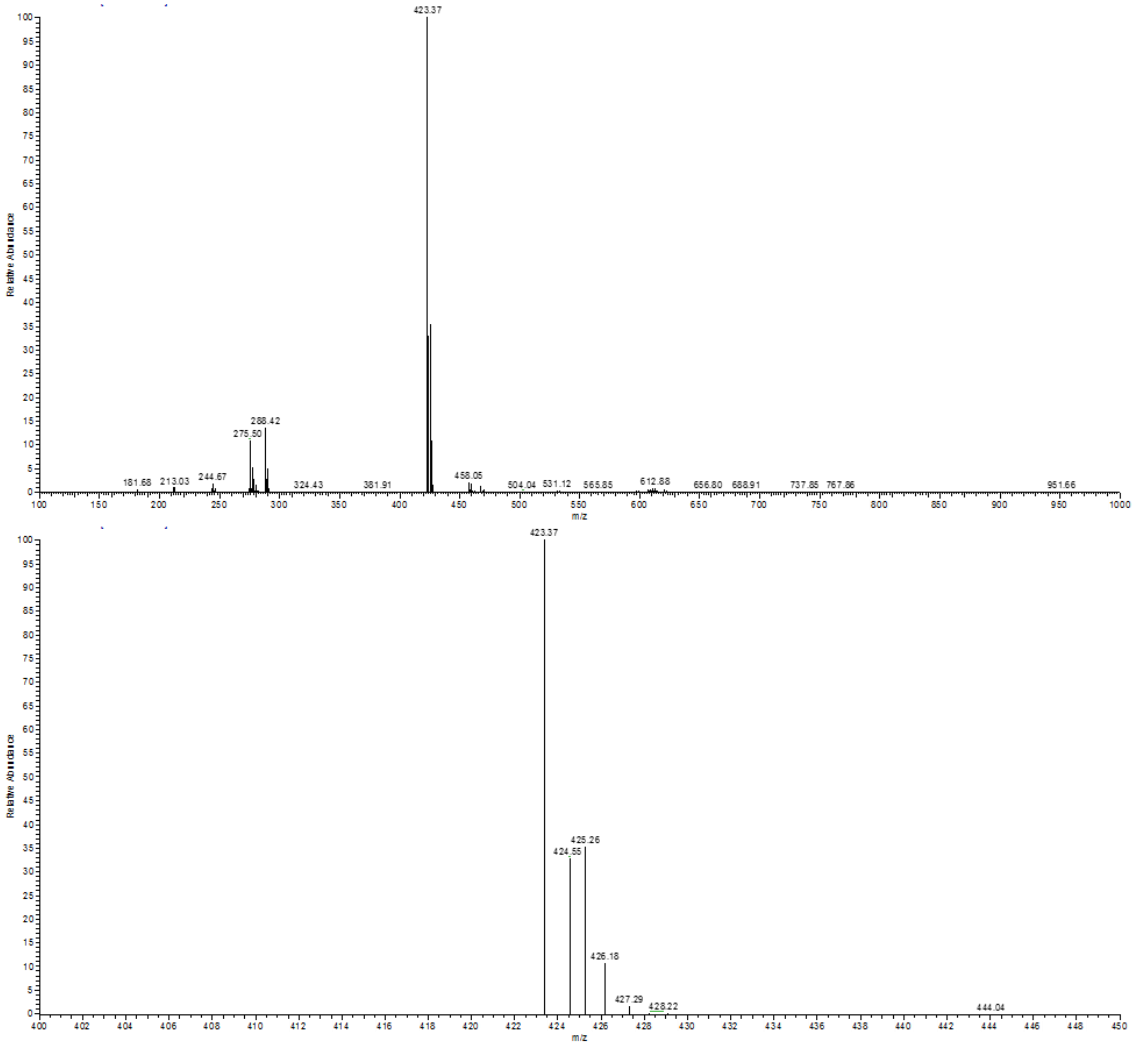

Figure S26. ESI−MS spectra (positive ion mode in CH_3OH) of **4**. The most intense signal is at m/z ($Cu(phen)_2$) = 423.37 (calcd: 423.37).

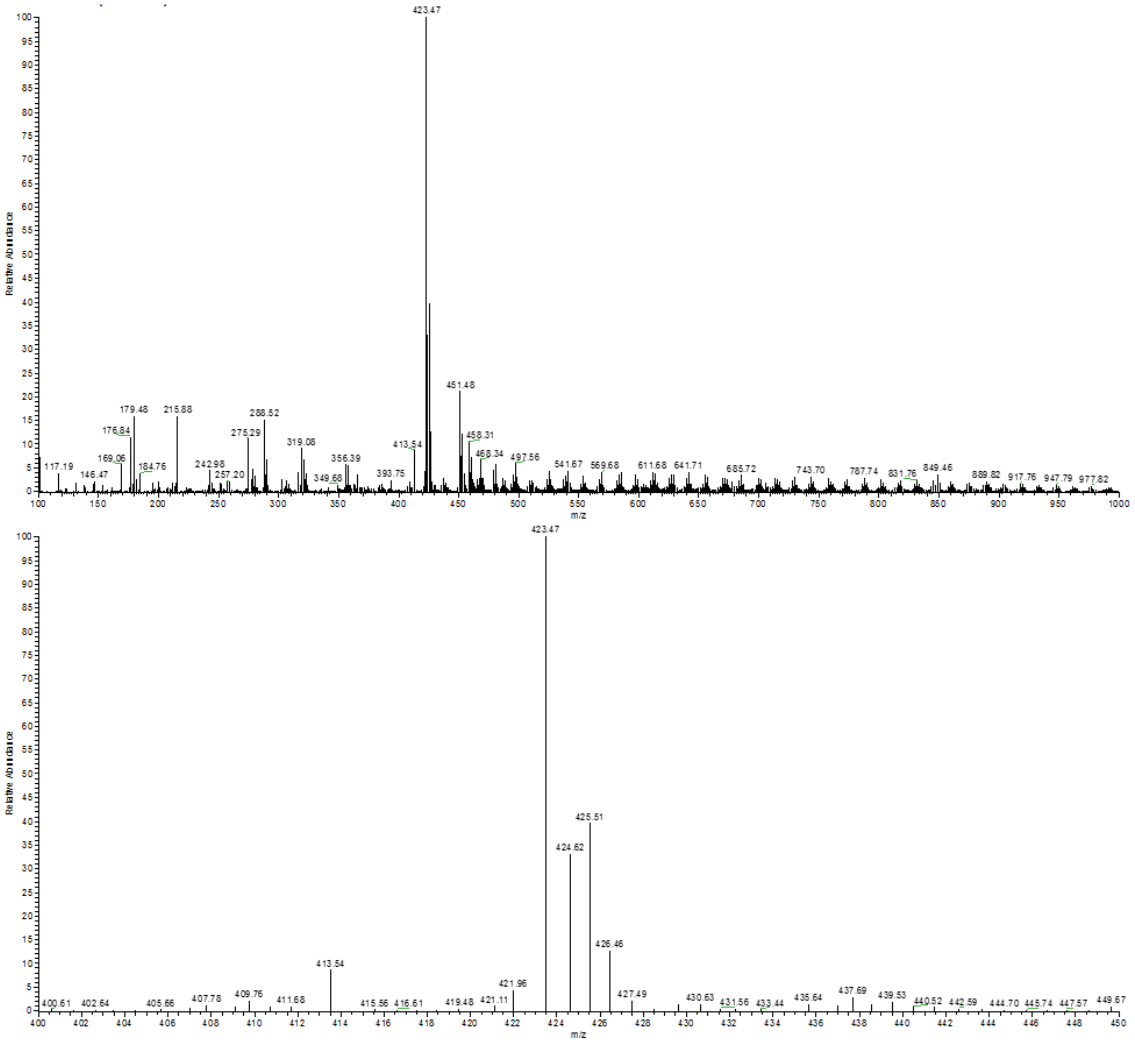

Figure S27. ESI−MS spectra (positive ion mode in CH_3OH) of the surface compounds isolated from DMSO treatment of the post-electrolysis **4** electrode. The most intense signal is at m/z ($Cu(phen)_2$) = 423.47 (calcd: 423.37).

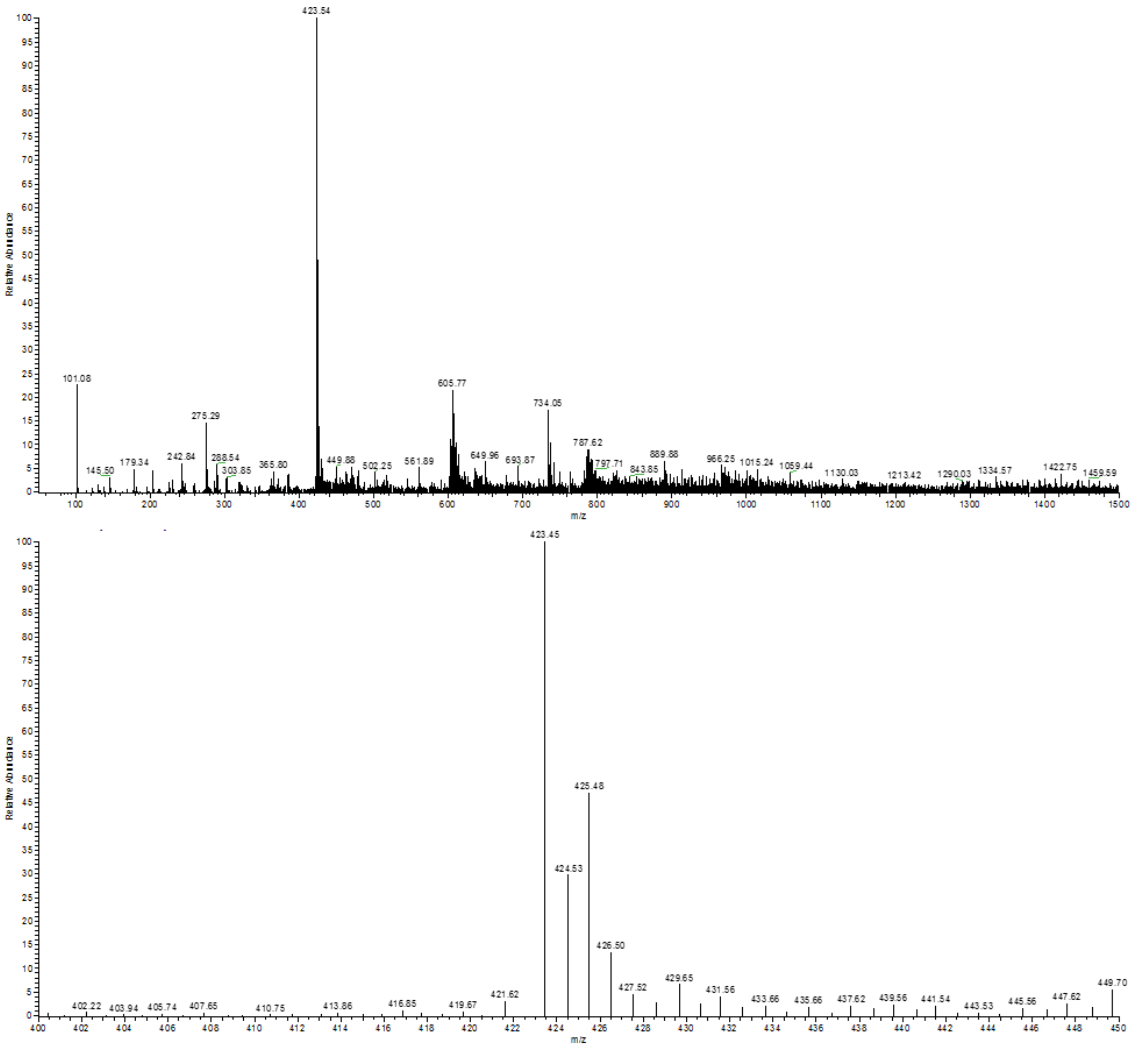

Figure S28. ESI−MS spectra (positive ion mode in CH_3OH) of the surface compounds isolated from DMSO treatment of $CuCl_2$-carbon paper electrode after added phen. The most intense signal is at m/z ($Cu(phen)_2$) = 423.47 (calcd: 423.37).

Table S19. Faradaic efficiencies toward different products produced during CO_2 reduction with 1.0 mM $CuCl_2$ as the pre-catalyst. Electrolysis was conducted in a CO_2-saturated 0.1 M $KHCO_3$ electrolyte at an applied potential of −1.3 V_{RHE} for 2 h.

Entry	FE (%)											*j*
	H_2	CO	HCOOH	CH_4	C_2H_4	C_2H_6	C_2H_5OH	C_3H_6	C_3H_7OH	C_{2+}	Total	(mA/cm^2)
1	63.5	6.3	12.8	0.3	6.4	0.1	0.4	0.1	1.2	8.2	91.1	14.5
2[a]	35.4	5.9	21.1	0.2	28.5	0.1	1.6	0.1	1.6	31.9	94.5	8.7
3	62.5	6.5	11.5	0.3	6.7	0.1	0.5	0.1	1.2	8.2	89.4	14.2
4[b]	56.8	6.1	8.8	0.1	8.4	0.1	8.0	0	1.3	17.8	89.6	4.2

[a] After experiment in entry 1, replace 0.1M CO_2-saturated $KHCO_3$ electrolyte with 1.0 mM phen.

[b] After experiment in entry 1, replace 0.1M CO_2-saturated $KHCO_3$ electrolyte with 1.0 mM *N*-tolyl pyridinium chloride.

Table S20. Faradaic efficiencies toward different products produced during CO_2 reduction added ligands. Electrolysis was conducted in a CO_2-saturated 0.1 M $KHCO_3$ electrolyte at an applied potential of −1.3 V_{RHE} for 2 h.

Pre-catalyst	FE (%)											*j*
	H_2	CO	HCOOH	CH_4	C_2H_4	C_2H_6	C_2H_5OH	C_3H_6	C_3H_7OH	C_{2+}	Total	(mA/cm^2)
$CuCl_2$+1.0 mM phen	23.5	25.7	13.5	0.8	25.9	0.4	1.3	0.1	0.2	27.9	91.4	4.5
$CuCl_2$+3.0 mM phen	18.8	38.6	20.1	2.3	16.1	0.1	1.5	0	0	17.7	97.5	2.9
$CuCl_2$+3.0 mM phen	11.9	44.9	25.6	8.3	7.1	0	2.1	0	0	9.2	99.0	2.2
$CuCl_2$+1.0 mM (5-py-phen)Cl	34.4	4.7	8.5	0.4	29.7	4.4	9.8	0.1	3.3	47.3	95.3	9.3
$CuCl_2$+3.0 mM (5-py-phen)Cl	25.4	15.5	12.7	2.3	29.0	2.0	10.1	0	1.1	42.2	98.1	5.4
$CuCl_2$+5.0 mM (5-py-phen)Cl	16.1	20.2	14.9	5.8	28.9	0.5	10.8	0	0.4	40.6	97.6	3.4
4+1.0 mM phen	7.1	21.7	2.8	18.1	44.6	0	2.2	0	0	46.8	96.5	3.7
6+1.0 mM (5-py-phen)Cl	12.0	26.6	13.5	9.7	12.9	0.4	15.3	0.1	3.5	32.2	95.7	3.1
$CuCl_2$+1.0 mM *N*-tolyl pyridinium chloride	41.7	9.2	9.5	1.2	20.6	0.2	7.4	0	1.2	29.4	91.0	3.8

Table S21. Faradaic efficiencies toward different products produced during CO_2 reduction with 1.0 mM **4** as the pre-catalyst. Electrolysis was conducted in a CO_2-saturated 0.1 M $KHCO_3$ electrolyte at an applied potential of −1.3 V_{RHE} for 2 h.

Entry	FE (%)											*j*
	H_2	CO	HCOOH	CH_4	C_2H_4	C_2H_6	C_2H_5OH	C_3H_6	C_3H_7OH	C_{2+}	Total	(mA/cm^2)
1	7.5	12.5	4.5	2.4	65.8	0.1	2.6	0.1	1.2	69.8	96.7	6.4
2	7.0	13.4	4.3	2.5	68.3	0.1	2.4	0.1	1.1	72.0	99.2	6.7
3	7.9	13.4	4.6	2.3	66.5	0.1	2.9	0.1	1.2	71.7	99.0	6.7
4[a]	60.3	16.4	6.9	5.5	6.4	0.2	0.1	0.4	0	7.1	96.2	3.2
5[b]	25.1	19.4	23.3	9.4	16.6	0	0.3	0	0	16.9	94.1	2.1
6[c]	9.2	15.3	4.2	2.2	62.3	0.1	2.5	0.1	1.0	66.0	96.9	6.9

[a] After experiment in entry 1, replace 0.1 M CO_2-saturated $KHCO_3$ electrolyte.

[b] After experiment in entry 2, replace 0.1 M CO_2-saturated $KHCO_3$ electrolyte with 1.0 mM phen.

[c] After experiment in entry 3, replace 0.1 M CO_2-saturated $KHCO_3$ electrolyte with 1.0 mM **4**.

References

1. Michels, T. D.; Rhee, J. U.; Vanderwal, C. D., Synthesis of δ-Tributylstannyl-α,β,γ,δ-Unsaturated Aldehydes from Pyridines. *Org. Lett.* **2008,** *10* (21), 4787-4790.
2. Han, Z.; Kortlever, R.; Chen, H. Y.; Peters, J. C.; Agapie, T., CO_2 Reduction Selective for C>/=2 Products on Polycrystalline Copper with N-Substituted Pyridinium Additives. *ACS Cent. Sci*. **2017**, *3* (8), 853-859.
3. N. Anitha, R. Balamurugan and M. Palaniandavar, J. Colloid Interf. Sci. 2011, 362, 243;
4. V. Leandri, Q. Daniel, H. Chen, L. Sun, J. M. Gardner and L. Kloo, Inorg. Chem. 2018, 57, 4556.
5. G. Murphy, P. Nagle, B. Murphy and B. Hathaway, J.Chem. Soc., Dal. Trans. 1997, 2645.
6. L. Lu, S. Qin, P. Yang and M. Zhu, Acta Crystallograph. 2004, 60, m574.
7. P. P. Laine, I. Ciofini, P. Ochsenbein, E. Amouyal, C. Adamo and F. Bedioui, Chem. Eur. J. 2005, 11, 3711.
8. Sheldrick, G. M., A short history of SHELX. *Acta Crystallogr. A.* **2008,** *64* (1), 112-122.
9. Dolomanov, O. V.; Bourhis, L. J.; Gildea, R. J.; Howard, J. A.; Puschmann, H., $OLEX_2$: a complete structure solution, refinement and analysis program. *J. Appl. Crystallogr.* **2009,** *42* (2), 339-341.
10. Wang, J.; Gan, L.; Zhang, Q.; Reddu, V.; Peng, Y.; Liu, Z.; Xia, X.; Wang, C.; Wang, X., A Water-Soluble Cu Complex as Molecular Catalyst for Electrocatalytic CO_2 Reduction on Graphene-Based Electrodes. *Adv. Energy Mater.* **2019,** *9* (3), 1803151.
11. Weng, Z.; Jiang, J.; Wu, Y.; Wu, Z.; Guo, X.; Materna, K. L.; Liu, W.; Batista, V. S.; Brudvig, G. W.; Wang, H., Electrochemical CO_2 Reduction to Hydrocarbons on a Heterogeneous Molecular Cu Catalyst in Aqueous Solution. *J. Am. Chem. Soc.* **2016,** *138* (26), 8076-8079.
12. Kusama, S.; Saito, T.; Hashiba, H.; Sakai, A.; Yotsuhashi, S., Crystalline Copper(II) Phthalocyanine Catalysts for Electrochemical Reduction of Carbon Dioxide in Aqueous Media. *ACS Catal.* **2017,** *7* (12), 8382-8385.
13. Balamurugan, M.; Jeong, H.-Y.; Choutipalli, V. S. K.; Hong, J. S.; Seo, H.; Saravanan, N.; Jang, J. H.; Lee, K.-G.; Lee, Y. H.; Im, S. W.; Subramanian, V.; Kim, S. H.; Nam, K. T., Electrocatalytic Reduction of CO_2 to Ethylene by Molecular Cu-Complex Immobilized on Graphitized Mesoporous Carbon. *Small* **2020,** *16* (25), 2000955.
14. Bose, P.; Mukherjee, C.; Kumar Golder, A., Reduction of CO_2 to Value‐Added Products on a Cu(II)‐Salen Complex Coated Graphite Electrocatalyst. *ChemistrySelect* **2020,** *5* (29), 9281-9287.
15. Yang, B.; Chen, L.; Xue, S.; Sun, H.; Feng, K.; Chen, Y.; Zhang, X.; Xiao, L.; Qin, Y.; Zhong, J.; Deng, Z.; Jiao, Y.; Peng, Y., Electrocatalytic CO_2 reduction to alcohols by modulating the molecular geometry and Cu coordination in bicentric copper complexes. *Nat. Commun.* **2022,** *13* (1), 1-13.

16. Bose, P.; Mukherjee, C.; Golder, A. K., A NiII complex of the tetradentate salen ligand H_2LNH_2 comprising an anchoring -NH_2 group: synthesis, characterization and electrocatalytic CO_2 reduction to alcohols. *Inorg. Chem. Front.* **2019,** *6* (7), 1721-1728.
17. Gonglach, S.; Paul, S.; Haas, M.; Pillwein, F.; Sreejith, S. S.; Barman, S.; De, R.; Müllegger, S.; Gerschel, P.; Apfel, U.-P.; Coskun, H.; Aljabour, A.; Stadler, P.; Schöfberger, W.; Roy, S., Molecular cobalt corrole complex for the heterogeneous electrocatalytic reduction of carbon dioxide. *Nat. Commun.* **2019,** *10* (1), 3864.
18. De, R.; Gonglach, S.; Paul, S.; Haas, M.; Sreejith, S. S.; Gerschel, P.; Apfel, U.-P.; Vuong, T. H.; Rabeah, J.; Roy, S.; Schöfberger, W., Electrocatalytic Reduction of CO_2 to Acetic Acid by a Molecular Manganese Corrole Complex. *Angew. Chem., Int. Ed.* **2020,** *59* (26), 10527-10534.
19. Liu, Y.; Fan, X.; Nayak, A.; Wang, Y.; Shan, B.; Quan, X.; Meyer, T. J., Steering CO_2 electroreduction toward ethanol production by a surface-bound Ru polypyridyl carbene catalyst on N-doped porous carbon. *Proc. Natl. Acad. Sci. U. S. A.* **2019**. 116, 26353-26358.